line capable of differentiating into trophoblastic cell lineages other than somatic cells [3]. It has been revealed that 6E2 reacts with not only human ECs, including NCR-G2 and 3 cells, but also other germ cell tumors, as well as normal human germ cells such as spermatogonia and oocytes [6]. Although a previous study reported that 6E2 immunoprecipitates a cell surface protein having a molecular weight of approximately 80 kDa from ^{125}I-labeled NCR-G3 cells, the specific antigen recognized by 6E2 still remains unknown. To characterize the antigen specificity of 6E2, we examined the reactivity of the Mab with other cell lines using several distinct methods. In this paper, we present evidence that 6E2 recognizes SSEA-4 carried by sialylGb5. Using 6E2, we determined the localization of SSEA-4 in "living" mouse preimplantation embryos and observed its preferential localization in interface between blastomeres.

Materials and methods

Cells, antibodies, and animals. The human renal carcinoma cell line ACHN was purchased from American Type Culture Collection. The African green monkey kidney cell line Vero was a gift from Dr. T. Takeda of Department of Infectious Diseases Research, National Children's Medical Research Center, Tokyo, Japan. Cells were maintained in Dulbecco's modified Eagle's minimum essential medium (DMEM) (Sigma Chem., St. Louis, MO) supplemented with 10% fetal bovine serum (FBS) (JRH Bioscience, Lenexa, KS). The human EC cell line NCR-G2 [3] was cultured in a 1:1 mixture of DMEM and Ham's F12 medium (DMEM/F12) (Invitrogen Gibco, Carlsbad, CA) supplemented with 10% FBS(JRH Bioscience), non-essential amino acid solution (NEAA) (Invitrogen Gibco), and Insulin-Transferin-Sodium Selenite media (Invitrogen Gibco). The cynomolgus monkey ES cell line CMK-6 [7] were provided by Dr. Yasushi Kondo of Mitsubishi Tanabe Pharma Corporation. ES cells were grown on mouse embryonic fibroblast feeder cells that were inactivated by gamma-irradiation in DMEM/F12 supplemented with 20% Knockout™ Serum Replacement, 2 mM Glutamax-I, 1% NEAA, 50 units/ml penicillin, 50 μg/ml streptomycin, 0.1 mM 2-mercaptoethanol, 1% sodium pyruvate, and 5 ng/ml bFGF (all from Invitrogen GIBCO). The cultures were performed at 37 °C in a 5% CO_2 incubator. The human venous blood from a healthy consenting volunteer was drawn in a heparin-coated syringe. The blood was spun at 3000 rpm for 15 min and human red blood cells (hRBCs) were washed three times in phosphate buffered saline (PBS).

The conjugation of affinity-purified 6E2 (mouse IgG_3, κ) [6] to the fluorescence reagent was performed with an Alexa Fluor® 488 monoclonal antibody labeling kit (Molecular Probes, Eugene, OR.) according to the manufacturer's instructions. The anti-SSEA-4 Mabs used in this study were Raft.2 [8] and MC813-70 (R&D Systems, Inc Minneapolis, MN). Alexa Fluor® 488 goat anti-mouse IgG and Streptavidin Alexa Fluor® 568 were purchased from Molecular probes.

BDF_1 mice were purchased from Clea Japan (Tokyo, Japan).

TLC immunostaining of GSLs. TLC immunostaining of GSLs from cultured cells and hRBCs was performed as previously described [9]. Reference GSLs were purchased from Matlayer, Inc. (Pleasant Gap, PA). SialylGb5 was purified from ACHN cells by preparative TLC. Purified GM1 b was kindly provided by Dr. Nakamura of RIKEN, Saitama, Japan [10].

Flow cytometry. Cells were harvested and incubated with a primary antibody (1 μg/ml) for 1 h on ice, followed by treatment with fluorescein isothiocyanate-conjugated goat anti-mouse immunoglobulins (Jackson Immunoresearch Laboratories, Inc., West Grove, PA) at a dilution of 1:50 and analyzed with an EPICS-XL flow cytometer (Beckman Coulter, Inc, Miami, FL).

Dot blot analysis. Purified sialylGb5 was serially diluted (0.1–60 ng) and vacuum blotted onto a PVDF membrane by using a 96-well format dot blot apparatus (Bio-Rad Laboratories, Richmond, CA). The membrane was immunostained with the Mab 6E2 or MC813-70 (0.5 μg/ml) according to a previously described procedure [9]. The antibodies that bound to the membranes were visualized with ECL-plus Western Blotting Detection Reagents (GE Healthcare UK Ltd, Buckinghamshire, UK) and scanned with a LAS-1000 luminescent imaging analyzer (Fujifilm, Tokyo, Japan). Scanned images were analyzed using the software Image Gauge with which the LAS-1000 was equipped.

Indirect immunostaining of cynomolgus monkey ES cells. Cells were grown on a glass-bottomed dish (IWAKI) for 3 days and then these cells were fixed for 30 min with 4% paraformaldehyde in PBS and permeabilized with 0.2% Triton X-200 in PBS for 20 min. Subsequently, the cells were washed three times with PBS for 5 min and blocked with 5% normal goat serum in PBS for 30 min. The fixed cells were incubated with anti-SSEA-4 antibodies or isotype-matched mouse IgG at a dilution of 1:300 for 2 h, followed by incubation with Alexa Fluor® 488-conjugated goat anti-mouse IgG at a dilution of 1:300 for 30 min. DAPI was used for counter staining of nuclei.

Immunostaining of mouse preimplantation embryos. Mouse preimplantation embryos were collected from superovulated mice. Seven-week-old BDF1 female mice were induced to superovulate with intraperitoneal injections of pregnant mare's serum gonadotropin (ASKA Pharmaceutical co., Ltd., Tokyo, Japan) (5 IU) and human chorionic gonadotropin (hCG) (ASKA Pharmaceutical co) (5 IU) 48 h apart and mated with individual BDF1 male mice after the hCG injection. The 2-cell, the 8-cell, and the morula stage embryos were flushed out from oviducts at 36, 60, and 72 h after the hCG injection, respectively. Animals were treated according to the institutional animal care and use guidelines of National Research Institute for Child Health and Development.

Embryos immediately after being collected and those prefixed with 2% paraformaldehyde in Hepes buffered saline were incubated in 30 μl drops of M16 medium containing 0.45 μg of Alexa Fluor® 488-conjugated 6E2 for 1 h or biotinylated MC813-70 for 1 h, treated with streptavidin Alexa Fluor® 568 diluted 1:300, and then they were washed three times in 30 μl drops of M16 medium. All staining steps were carried out at 37 °C in a CO_2 incubator for fresh embryos and at 4 °C for fixed embryos. The stained embryos were placed in drop of a M16 medium on glass-bottomed dishes (IWAKI, Tokyo, Japan), and were observed with a LSM510 Zeiss Confocal laser-scanning microscope (Carl Zeiss, Thornwood, NY) to obtain a field of view of the embryo only with a 40× objective lens.

Results and discussion

6E2 specifically binds to sialylGb5

In order to examine whether the 80 kDa membrane protein is recognized by 6E2, we performed a Western analysis of the cell lysates or their immunoprecipitates with 6E2. Since no significant signal was detected on the blot (data not shown), we examined TLC immunostaining of GSLs extracted from several 6E2-positive cell lines. ACHN cells showed the expression of comparable amounts of Gb3, Gb4, Gb5, and sialylGb5, whereas Vero cells and NCR-G2 cells expressed predominantly Gb3 (Fig. 1A). TLC immunostaining analysis revealed that 6E2 binds to a major slow-migrating GSL extracted from these three cell lines. The slow-migrating GSL was identified as sialylGb5, defined by the Mab Raft.2. We observed that 6E2 bound to sialylGb5 (LKE-antigen) of hRBCs [13] (Fig. 1B). Finally, we examined the reactivity of 6E2 with purified GSLs and found that the Mab reacts with purified sialylGb5, but not purified GM1 b (Fig. 1C). These results indicate that 6E2 specifically binds to sialylGb5 and thus is an anti-SSEA-4

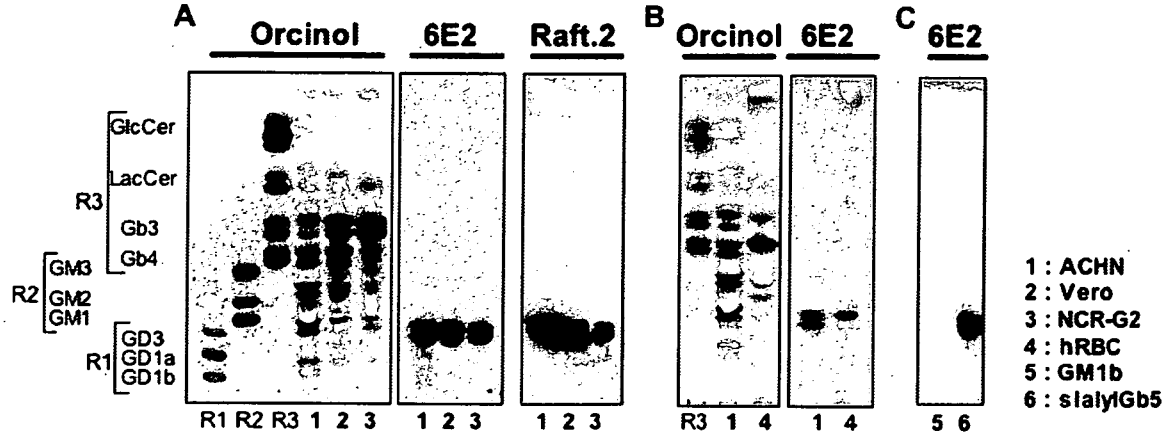

Fig. 1. TLC immunostaining of GSLs prepared from cultured cells and hRBCs. GSLs extracted from cultured cells and hRBCs or purified GSLs were separated by TLC in a solvent system of chloroform/methanol/water containing 0.2% $CaCl_2$ (5:4:1, v/v/v). Plates were chemically stained with orcinol-sulfurnic acid or were immunostained with 6E2 and Raft.2. Lane 1, ACHN; Lane 2, Vero; Lane 3, NCR-G2; Lane 4, hRBCs; Lane 5, GM1b; Lane 6, sialylGb5. Reference markers used were disialosyl gangliosides of GD3, GD1a, and GD1b (R1), monosialosyl gangliosides of GM3, GM2, and GM1 (R2), and neutral GSLs of GlcCer, LacCer, Gb3, and Gb4 (R3). The nomenclature for GSLs follows the recommendations [11] of the IUB, and the ganglioside nomenclature of Svennerholm [12] was used.

Mab. The 80 kDa protein might be associated with sialylGb5 in NCR-G3 cells and thus co-immunoprecipitated by 6E2.

Comparison of reactivity to sialyl Gb5 between 6E2 and MC813-70

MC813-70 established by immunizing with human EC cell lines has been most widely used as an anti-SSEA-4 antibody (mouse IgG_3, κ) [14]. Therefore we compared the reactivities of the Mabs 6E2 and MC813-70 by flow cytometry and dot-blot immunostaining. The fluorescence intensity obtained with 6E2 was stronger than that with MC813-70 in each cell line and hRBCs (Fig. 2A). A recent flow cytometric study showed that MC813-70 strongly stains hRBCs, but other anti-sialyGb5 Mabs do not [15]. However, our data indicate that 6E2 is more reactive than MC813-70. Next we compared the reactivity of the two

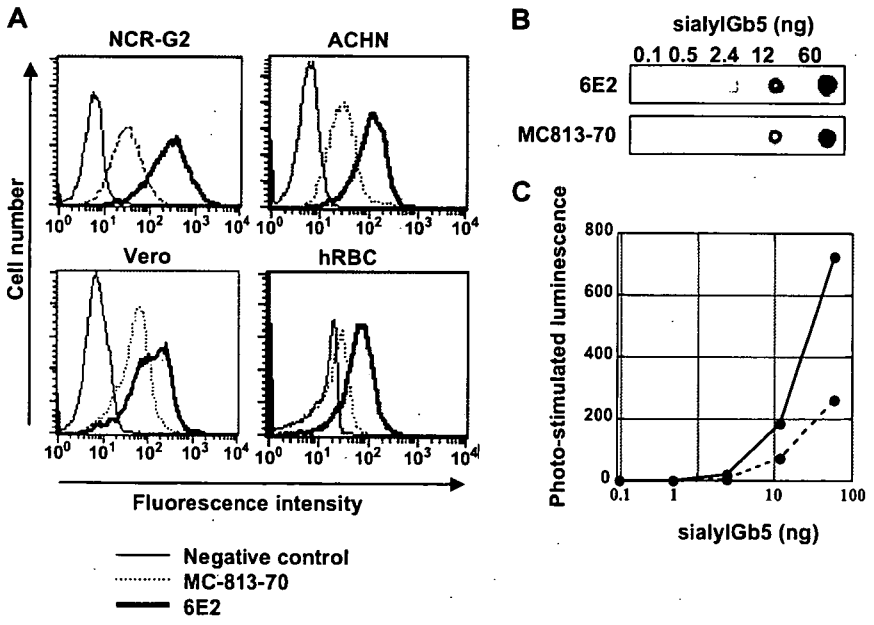

Fig. 2. Reactivity of 6E2 and MC813-70 with sialylGb5. (A) Flow cytometric analysis of SSEA-4-positive cells with 6E2. NCR-G2 cells, ACHN cells, Vero cells, and hRBCs were stained with 6E2 (bold line) or MC813-70 (dotted line) and with a FITC-conjugated secondary antibody and analyzed by flow cytometry. (B) An image of the dot-blot immunostaining of sialylGb5 obtained with a LAS-1000 luminescent imaging analyzer. (C) Measurement of antibodies bound (6E2: solid line, MC813-70: broken line).

Mabs with that of sialylGb5 by dot-blot immunostaining. Serially diluted sialylGb5 was dot-blotted onto a PVDF membrane, and the membrane was immunostained with the two Mabs. Both 6E2 and MC813-70 bound to more than 12 ng of sialylGb5, but the signals induced by 6E2 were stronger than those induced by MC813-70 (Fig. 2B,C). Thus, in addition to the flow cytometric analysis, the reactivity of 6E2 with sialylGb5 was stronger than that of MC813-70 by dot-blot immunostaining.

SSEA-4 Immunostaining of cynomolgus monkey ES cells

To confirm whether Mab 6E2 reacts with SSEA-4 on monkey ES cells, we performed an indirect immunofluorescence staining of cynomolgus monkey ES cells with Mab 6E2 and MC813-70. Mab 6E2 reacted with monkey ES cells (Fig. 3A) as well as MC-813-70 did (Fig. 3B). No difference in staining patterns of SSEA-4 between the two Mabs was observed. Mab 6E2 certainly stained SSEA-4 on monkey ES cells.

SSEA-4 immunostaining of "living" mouse preimplantation embryos without fixation

During early embryogenesis in mice, SSEA-4 had been reported to be expressed in fertilized eggs with levels gradually increasing to the morula stage and then decreasing [5]. Thus we examined the expression and distribution of SSEA-4 in preimplantation mouse embryos by immunostaining with both 6E2 and MC813-70. Both Mabs evenly stained the whole surface membranes of fixed mouse embryos, and no difference in staining pattern between the two was observed (data not shown). In order to perform a time-course of SSEA-4 distribution in a viable state, we performed immunostaining of preimplantation embryos without fixation.

3D-images of the 6E2 staining pattern obtained by confocal laser scanning microscopic observation clearly showed the localization of SSEA-4 on mouse preimplantation embryos. Two-cell embryos showed patches of SSEA-4 over the whole surface membrane with some accumulation at the interface between blastomeres (Fig. 4A). In 8-cell embryos, the amount accumulated at interfaces was further increased, as if planer membranes separate each blastomere, and some large patches were internalized but others were left on the surface membranes (Fig. 4B). The amount of SSEA-4 concentrated at the interfaces in morula was not as significant as in 8-cell embryos but still clearly observed and some patches were internalized (Fig. 4C).

2D-images of embryos stained with 6E2 showed a marked accumulation of SSEA-4 at the interfaces between blastomeres (Fig. 4D–F). These results suggest that sialylGb5 actively moves during development and tends to accumulate where blastomeres come into contact with each other.

Interestingly, however, the staining pattern of SSEA-4 using MC813-70 was different from that using 6E2. MC813-70 evenly stained the surface and the interface between blastomeres of 2-cell embryos with patches (Fig. 4G), and the amount of SSEA-4 at interfaces was not significant (Fig. 4J). In 8-cell embryos, there were patches of SSEA-4 in the central area of the outer surface of each blastomere (Fig. 4H, indicated by arrows), but the 2D-image showed that clustering also occurred at surfaces facing blastocoels (Fig. 4K, indicated by arrowheads). In morula embryos, SSEA-4 was distributed on the surface in patches and was enriched at the boundaries between blastomeres on the outer surface (Fig. 4I,L).

It remains unclear why the pattern of staining of mouse preimplantation embryos differs between 6E2 and MC813-70. The composition of fatty acids in GSLs influences the binding of antibodies [16,17] or bacterial toxins [18]. SialylGb5 recognized by the two MAbs might differ in composition of fatty acids, resulting in different immunostaining patterns. It was reported that the clustering of sialylGb5 by a Mab induces the activation of sialylGb5-associated kinases in raft microdomains of human mammary carcinoma cells, leading to downstream signaling [19,20]. The clustering of sialyGb5 by 6E2 on preimplantation mouse embryos may also induce the activation of some kinases, followed by downstream signaling. Recently, Comisky et al. suggested that lipid rafts and their associated molecules are spatiotemporally positioned to play a critical role in preimplantation developmental events [21]. The patches or clusters of sialylGb5 shown in our study suggest the presence of lipid rafts containing sialylGb5 on mouse embryos.

Fig. 3. Indirect immunostaining of cynomolgus monkey ES cell line CMK-6 with 6E2 and MC813-70. The CMK-6 cells were stained with 6E2 (A), MC813-70 (B), or isotype-matched mouse IgG (C), and visualized with secondary antibodies (green), followed by counterstaining of nuclei with DAPI (blue). Scale bars = 200 μm.

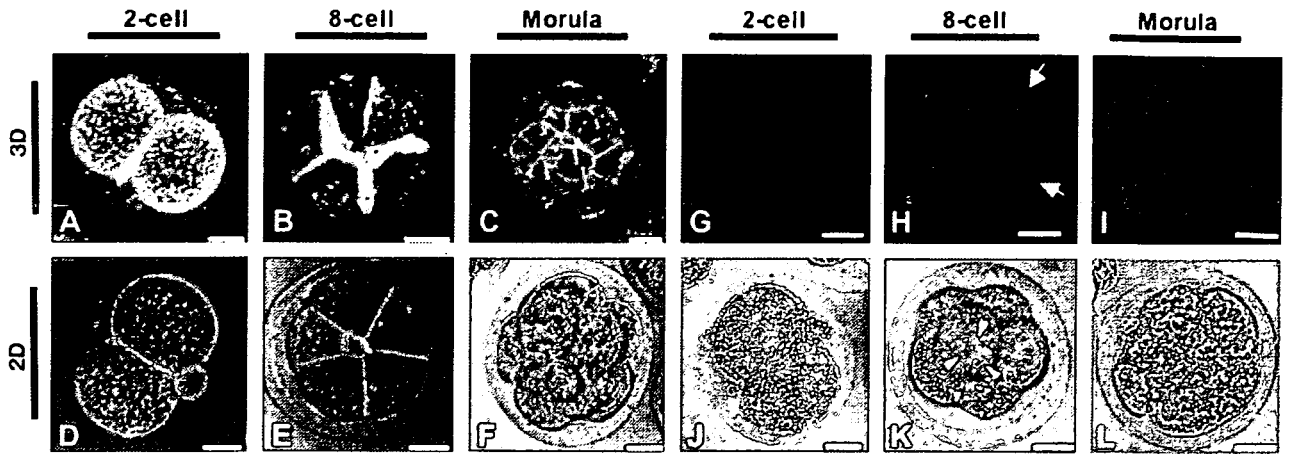

Fig. 4. Immunostaining of SSEA-4 on mouse preimplantation embryos with 6E2 and MC813-70. The embryos at the 2-cell (A, D, G, J), the 8-cell (B, E, H, K), and the morula (C, F, I, L) stages were stained with 6E2 (green) or MC813-70 (red). The panels designated 3D (A, B, C, G, H, I) are three-dimensional images reconstructed by stacking optical slice images using LSM software and the panels designated 2D (D, E, F, J, K, L) are an overlay of a fluorescent image and a differential interference contrast micrograph. Scale bars = 20 μm.

6E2 has high affinity for sialylGb5 and can be effectively conjugated with fluorescence reagents, leading to excellent staining of SSEA-4 in the surface membrane of "living" mouse preimplantation embryos. 6E2 should be of use for research into lipid rafts in early development and of great advantage for the characterization of ES cells and EC cells.

Acknowledgments

We thank S. Yamauchi for her excellent secretarial work. This work was supported in part by grants from CREST of JST and the 3rd. term comprehensive 10-year-strategy for cancer control, Research on Children and Families, Research on Human Genome Tailor made and Research on Publicly Essential Drugs and Medical Devices, Health and Labour Sciences Research Grants from the Ministry of Health, Labour and Welfare of Japan and a grant from The Japan Leukemia Research Field.

References

[1] B. Mintz, K. Illmensee, Normal genetically mosaic mice produced from malignant teratocarcinoma cells, Proc. Natl. Acad. Sci. USA 72 (1975) 3585–3589.
[2] P.W. Andrews, I. Damjanov, D. Simon, G.S. Banting, C. Carlin, N.C. Dracopoli, J. Fogh, Pluripotent embryonal carcinoma clones derived from the human teratocarcinoma cell line Tera-2. Differentiation in vivo and in vitro, Lab Invest. 50 (1984) 147–162.
[3] J.F. Jun-ichi Hata, Eizaburo Ishii, Akihiro Umezawa, Yasuo Kokai, Yoshie Matsubayashi, Hiroshi Abe, Satoru Kusakari, Haruto Kikuchi, Taketo Yamada, Tatsuya Maruyama, Differntiation of human germ cell tumor cells *in vivo* and *in vitro*, Acta Histochem. Cytochem. 25 (1992) 563–576.
[4] J.S. Draper, C. Pigott, J.A. Thomson, P.W. Andrews, Surface antigens of human embryonic stem cells: changes upon differentiation in culture, J. Anat. 200 (2002) 249–258.
[5] T. Muramatsu, H. Muramatsu, Carbohydrate antigens expressed on stem cells and early embryonic cells, Glycoconj. J. 21 (2004) 41–45.
[6] T. Nakano, A. Umezawa, H. Abe, N. Suzuki, T. Yamada, S. Nozawa, J. Hata, A monoclonal antibody that specifically reacts with human embryonal carcinomas, spermatogonia and oocytes is able to induce human EC cell death, Differentiation 58 (1995) 233–240.
[7] M. Yamamoto, N. Tase, T. Okuno, Y. Kondo, S. Akiba, N. Shimozawa, K. Terao, Monitoring of gene expression in differentiation of embryoid bodies from cynomolgus monkey embryonic stem cells in the presence of bisphenol A, J. Toxicol. Sci. 32 (2007) 301–310.
[8] Y.U. Katagiri, K. Ohmi, C. Katagiri, T. Sekino, H. Nakajima, T. Ebata, N. Kiyokawa, J. Fujimoto, Prominent immunogenicity of monosialosyl galactosylgloboside, carrying a stage-specific embryonic antigen-4 (SSEA-4) epitope in the ACHN human renal tubular cell line-a simple method for producing monoclonal antibodies against detergent-insoluble microdomains/raft, Glycoconj. J. 18 (2001) 347–353.
[9] Y.U. Katagiri, N. Kiyokawa, K. Nakamura, H. Takenouchi, T. Taguchi, H. Okita, A. Umezawa, J. Fujimoto, Laminin binding protein, 34/67 laminin receptor, carries stage-specific embryonic antigen-4 epitope defined by monoclonal antibody Raft.2, Biochem. Biophys. Res. Commun. 332 (2005) 1004–1011.
[10] K. Nakamura, Y. Hashimoto, M. Suzuki, A. Suzuki, T. Yamakawa, Characterization of GM1b in mouse spleen, J. Biochem. (Tokyo) 96 (1984) 949–957.
[11] The nomenclature of lipids (recommendations 1976). IUPAC-IUB Commission on Biochemical Nomenclature, J. Lipid. Res. 19 (1978) 114–128.
[12] L. Svennerholm, Designation and schematic structure of gangliosides and allied glycosphingolipids, Prog. Brain Res. 101 (1994) XI–XIV.
[13] L.L. Cooling, K. Kelly, Inverse expression of P(k) and Luke blood group antigens on human RBCs, Transfusion 41 (2001) 898–907.
[14] L.H. Shevinsky, B.B. Knowles, I. Damjanov, D. Solter, Monoclonal antibody to murine embryos defines a stage-specific embryonic antigen expressed on mouse embryos and human teratocarcinoma cells, Cell 30 (1982) 697–705.
[15] L. Cooling, D. Hwang, Monoclonal antibody B2, a marker of neuroendocrine sympathoadrenal precursors, recognizes the Luke (LKE) antigen, Transfusion 45 (2005) 709–716.
[16] K. Iwabuchi, I. Nagaoka, Lactosylceramide-enriched glycosphingolipid signaling domain mediates superoxide generation from human neutrophils, Blood 100 (2002) 1454–1464.
[17] K. Iwabuchi, Y. Zhang, K. Handa, D.A. Withers, P. Sinay, S. Hakomori, Reconstitution of membranes simulating "glycosignaling

domain" and their susceptibility to lyso-GM3, J. Biol. Chem. 275 (2000) 15174–15181.
[18] A. Kiarash, B. Boyd, C.A. Lingwood, Glycosphingolipid receptor function is modified by fatty acid content. Verotoxin 1 and verotoxin 2c preferentially recognize different globotriaosyl ceramide fatty acid homologues, J. Biol. Chem. 269 (1994) 11138–11146.
[19] W.F. Steelant, Y. Kawakami, A. Ito, K. Handa, E.A. Bruyneel, M. Mareel, S. Hakomori, Monosialyl-Gb5 organized with cSrc and FAK in GEM of human breast carcinoma MCF-7 cells defines their invasive properties, FEBS Lett. 531 (2002) 93–98.
[20] S. Van Slambrouck, W.F. Steelant, Clustering of monosialyl-Gb5 initiates downstream signalling events leading to invasion of MCF-7 breast cancer cells, Biochem. J. 401 (2007) 689–699.
[21] M. Comiskey, C.M. Warner, Spatio-temporal localization of membrane lipid rafts in mouse oocytes and cleaving preimplantation embryos, Dev. Biol. 303 (2007) 727–739.

FEBS Letters 581 (2007) 4685–4690

Eye-open at birth phenotype with reduced keratinocyte motility in LGR4 null mice

Shigeki Kato[a,1], Yasuaki Mohri[a], Tsuyoshi Matsuo[a], Eisaku Ogawa[b], Akihiro Umezawa[c], Ryuhei Okuyama[b], Katsuhiko Nishimori[a,*]

[a] *Laboratory of Molecular Biology, Graduate School of Agricultural Science, Tohoku University, 1-1 Tsutsumidori-Amamiyamachi, Aoba-ku, Sendai 981-8555, Japan*
[b] *Department of Dermatology, Tohoku University Graduate School of Medicine, 2-1 Seiryo-machi, Aoba-ku, Sendai 980-8574, Japan*
[c] *National Research Institute for Child Health and Development, 2-10-1, Okura, Setagaya-ku, Tokyo 157-8535, Japan*

Received 30 July 2007; accepted 27 August 2007

Available online 4 September 2007

Edited by Ned Mantei

Abstract **We observed a consistent eye-open at birth (EOB) phenotype in mouse pups homozygous for a leucine-rich repeat containing G-protein coupled receptor 4 (*Lgr4*) allele deleting the whole transmembrane domain coding region. An in vitro wound-healing scratch assay showed notably reduced keratinocyte motility in the null mice. Phalloidin staining of F-actin in the eyelid epidermis was also reduced. We also generated keratinocyte-specific *Lgr4* deficient mice, circumventing the embryonic/neonatal lethality and kidney abnormalities. Most of the conditional *Lgr4* knockout mice showed the EOB phenotype. Thus, *Lgr4* might be a novel gene class regulating cell motility.**

Keywords: LGR4; GPR48; GPCR; Gene deletion mice; EOB; Keratinocyte

1. Introduction

Lgr4 (leucine-rich repeat containing G-protein coupled receptor 4) is one of the genes identified as novel G-protein coupled receptors (GPCRs) [1,2], designated *Lgr4–Lgr8*, from an EST database with high homology to glycoprotein hormone receptors including follicle-stimulating hormone receptor (FSHR) [3], luteinizing hormone/chorionic gonadotropin receptor (LH/CGR) [4,5] and thyroid-stimulating hormone receptor (TSHR) [6].

As *Lgr4* shows high homology with FSHR, LHR and THSR, this receptor has been thought to be involved in reproductive systems. Mazerbourg et al. reported the generation of *Lgr4* gene-interrupted mice using a gene-trapped ES cell line [7], in which the expression of *Lgr4* is severely attenuated by the insertion of the β-geo gene in an enhancer trap procedure [8]. They described the neonatal lethality of the null mice, but not the cause. Previously, we generated similar *Lgr4* knockout mice by completely removing exon18, which encodes the whole transmembrane domain of *Lgr4*, in order to eliminate the chance of receptor fragment localizing at the membrane or transmitting downstream signals [9]. In those *Lgr4* knockout mice, gross hypomorphic phenotypes developed in multiple tissues and organs, and the null mice showed hypoplastic kidneys with an increased concentration of plasm creatinine, which was strongly suspected to be the cause of the neonatal/embryonic lethality.

Recently, Mendive et al. as well as Hoshii et al. reported *Lgr4* gene-trap lines exhibiting defective postnatal development of the male reproductive tract [10,11], again in contrast to the embryonic/neonatal lethality seen in our *Lgr4* knockout mice on a 129Ola × C57BL/6 hybrid background [9]. In our *Lgr4* knockout mice it appeared that complete loss of the *Lgr4* gene would induce complete embryonic/neonatal lethality. As reported in our first paper, the typical phenotype of the *Lgr4* null mutants other than the kidney aberration was eye open at birth (EOB) with 100% penetrancy, strongly suggesting reduced keratinocyte proliferation and motility. Several studies have reported a strong relationship between a reduction in keratinocyte proliferation/motility and the EOB phenotype [12,13], and it has been suggested that *Lgr4* is essential for organ development and cancer cell invasion [10,11,14]. Additionally, a close relationship between cancer cell invasion and cell motility was reported, and it is well known that organ development requires cell motility [15,16]. We therefore suspected the existence of a close relationship between *Lgr4* and cell motility, and considered that common mechanisms might cause EOB and the other abnormalities observed in *Lgr4* null mice. In the present study we focused on the EOB phenotype in relation to the keratinocyte motility of the null mice.

We provide evidence that *Lgr4* has a role in keratinocyte motility. In addition, we succeeded in dissociating the EOB phenotype, first observed in all conventional *Lgr4* KO mice, from the kidney lesions and lethality using conditional *Lgr4* knockout mice crossed with K5-Cre transgenic mice.

*Corresponding author. Fax: +81 22 717 8883.
E-mail address: knishimo@mail.tains.tohoku.ac.jp (K. Nishimori).

[1]Present address: Department of Molecular Genetics, Institute of Biomedical Sciences, Fukushima Medical University, 1 Hikarigaoka, Fukushima 960-1295, Japan.

Abbreviations: LGR, leucine-rich repeat containing G-protein coupled receptor; GPCR, G-protein coupled receptor; FSHR, follicle-stimulating hormone receptor; LH/CGR, luteinizing hormone/chorionic gonadotropin receptor; TSHR, thyroid-stimulating hormone receptor; EOB, eye-open at birth; Arbp, acidic ribosomal phosphoprotein PO

0014-5793/$32.00
doi:10.1016/j.febslet.2007.08.064

2. Materials and methods

2.1. Histology

For the eyelid histology, the heads of the mice were fixed in 4% paraformaldehyde overnight. After dehydration, they were embedded in paraffin. Paraffin blocks were sectioned at 2–5 μm thickness and stained with H&E (hematoxylin–eosin) and Phalloidin-TRITC (tetramethyl rhodamine isothiocyanate) using standard procedures.

2.2. In vitro apoptosis cell test

Sections from around the eyelids of E15.5 mice were used for the detection of apoptotic cells. Samples were processed according to the protocol of In Situ Cell Death Detection Kit (Roche, Japan).

2.3. Keratinocyte primary culture

Primary keratinocytes were isolated from neonatal mice. The epidermis was separated from the dermis with 0.8 U/ml dispase (Roche) overnight at 4 °C. Keratinocytes were dissociated by trypsin for 5 min at 34 °C and plated onto dishes precoated with collagen type I. The cells were cultured in minimum essential medium supplemented with 4% Chelex (Bio-Rad, Hercules, CA)-treated fetal calf serum epidermal growth factor (10 ng/ml; Gibco BRL), and 0.05 mM $CaCl_2$ at 34 °C in an 8% CO_2 incubator. Under these conditions, keratinocytes are maintained in an immature state characterized by active proliferation. For all the experiments, the cells were used one week after plating.

2.4. In vitro migration assay

Keratinocytes derived from each genotype of neonatal mice were cultured until confluent. After scratching with plastic tips, the distance that the keratinocyte migrated was measured every 3 h. Each sample was counted at 16 points and the average distance was calculated.

2.5. Quantitative RT-PCR

Messenger RNA derived from wild-type and *Lgr4* null mice keratinocyte was subjected to cDNA synthesis by standard procedures. Quantitative RT-PCR assays were performed with the DNA Engine Opticon System (MJ Research, Japan) with a cycling profile as follows: at 95 °C for 2 min, 39 cycles at 95 °C for 5 s, at 61.4 °C for 30 s, and at 72 °C for 30 s. The genes and primer sets are shown in the supplementary material.

2.6. Generation of keratinocyte specific Lgr4 deficient mice

To generate *Lgr4* fx/fx mice without frt-Neo-frt cassette, an initially targeted *Lgr4* mutant [9] was mated with Flp deleter [17]. Mice with the keratinocyte-specific *Lgr4* deletion were generated by breeding keratin5-Cre (K5-Cre); *Lgr4* +/− mice with *Lgr4* fx/fx mice [18]. The genetic backgrounds were C57Bl/6 × 129Ola for *Lgr4* +/− and *Lgr4* fx/fx, and C57Bl/6 × C3H for K5-Cre. Primers for *Lgr4* genotyping are shown in the supplementary material.

2.7. Statistical evaluation

All experimental data are expressed as mean S.E.M. Statistical comparisons in all the physiological and laboratory data were made among the genotype groups using ANOVA followed by Student's *t*-test for individual comparisons. *P* values of <0.05 were considered significant.

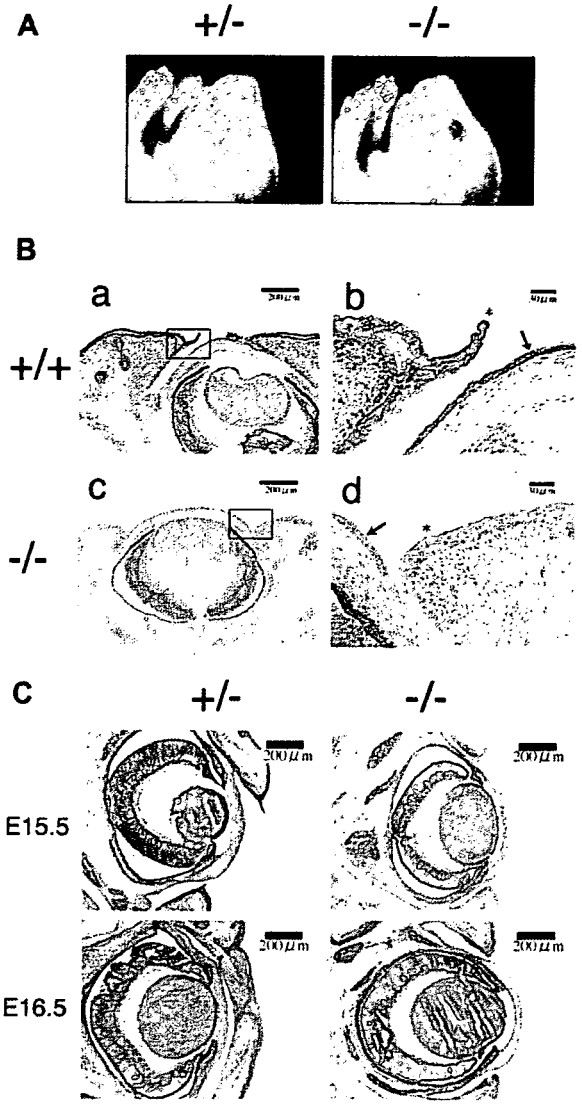

Fig. 1. *Lgr4* deficiency causes impairment in embryonic eyelid closure. (A) Left panel and right panel show morphology around eyes of *Lgr4* heterozygous (*Lgr4* +/−) and *Lgr4* null mice, respectively at postnatal day 0. (B) Eyelid sections prepared from E 15.5 wild-type (a, b) or null (c, d) mouse fetuses were immunostained with rabbit anti-LGR4 antibody (ab 12576, Abcam, USA), followed by HRP-conjugated second antibody. Asterisks show epithelial cell layer at the protruding tips of the growing eyelids, and arrows show the corneal epithelium layer. (C) Histological analysis (H&E staining) of E15.5 and E16.5 embryos.

3. Results

3.1. Lgr4 null mice show morphological abnormalities in the eyelids at E15.5

Lgr4 null mice showed some gross abnormalities. In wild-type mice during the embryonic stages E15.5 through E16.5, epithelial cells extended to the center of the eyes and finally became fused. The mice were then born with their eyelids fused, and the eyelids opened gradually by 12–14 days after birth. However, *Lgr4* null mice showed the EOB phenotype with 100% penetrance (Fig. 1A). Histological analysis of the wild-type mice followed by immunostaining showed a high expression level of *Lgr4* at the protruding tips of the eyelids and in the epithelial cells of the cornea at E15.5, but no expression was detected in the same areas of the null mice (Fig. 1B). As shown in Fig. 1C right, the eyelid closure was impaired in the null mice as compared to the heterozygous mice (Fig. 1C, left).

3.2. Proliferation and motility of keratinocytes from Lgr4 null mice

EOB has been reported as a typical phenotype reflecting keratinocyte proliferation/motility, which we then measured. No decrease in proliferating cells was detected in the eyelid epi-

thelium of the null mutants at E15.5 (data not shown). Since a reduction of the cytoplasmic accumulation of F-actin was observed with the EOB phenotype in some gene knockout studies [19,20], we stained the eyelid sections with phalloidin and found that there was less filamentous accumulation of F-actin at the margin of the eyelid epithelium, as shown in Fig. 2A. Furthermore, we examined the extent of keratinocyte proliferation in vitro using the incorporation of BrdU, but no significant difference between the wild-type and the *Lgr4* null mice was observed (date not shown). Next, the keratinocyte motility was measured by an in vitro migration assay. The lack of *Lgr4* was related to a reduction of the keratinocyte motility, and we observed a significant delay in healing 3 hours after scratching in the cells from the null mice (Fig. 2B and C). To further analyze other possible mechanisms responsible for EOB in addition to the reduced motility of the null mice, wild-type and *Lgr4* null fetuses at E15.5 were subjected to TUNEL assay to examine the extent of cell apoptosis around the eyelid tissues. However, neirther types of embryos showed any apoptotic cells (Fig. 2D).

These results suggest that the EOB observed in the null mice was not induced by an enhancement of apoptosis, and provide further evidence that *Lgr4* is a critical regulator for keratinocyte motility in the epidermal tissue of eyelids.

3.3. Quantitative RT-PCR of EOB related genes in keratinocytes from Lgr4 null mice

The disruption of *EGFR*, *EGF*, *TGF-α*, *ADAM17*, *c-jun*, *ActivinA* and *ActivinB* genes has been reported to cause EOB. We measured the expression levels of these genes in mRNA prepared from wild-type and *Lgr4* null keratinocytes, but did not detect any significant differences in their expression levels (Fig. 3). In addition, the expression level of EGFR around the eyelid at E15.5 in the null mutants was normal (Supplementary Fig. S1). The phosphorylation of EGFR around the eyelid at E15.5 was examined in wild-type and *Lgr4* null mice by immunostaining, but no significant difference was observed (date not shown). The phosphorylation of ERK and JNK of the same samples also showed no difference (Supplementary Fig.S1).

3.4. Generation of keratinocyte-specific Lgr4 deficient mice

As mentioned above, the EOB phenotype observed in *Lgr4* null mice was suspected to be closely related to reduced keratinocyte motility. We previously reported that *Lgr4* null mice showed renal hypoplasia [9]. To separate the EOB phenotype from the renal hypoplasia observed in *Lgr4* null mice, we additionally generated keratinocyte-specific *Lgr4* deficient mice (*Lgr4* conditional knockout mice) as described in Section 2

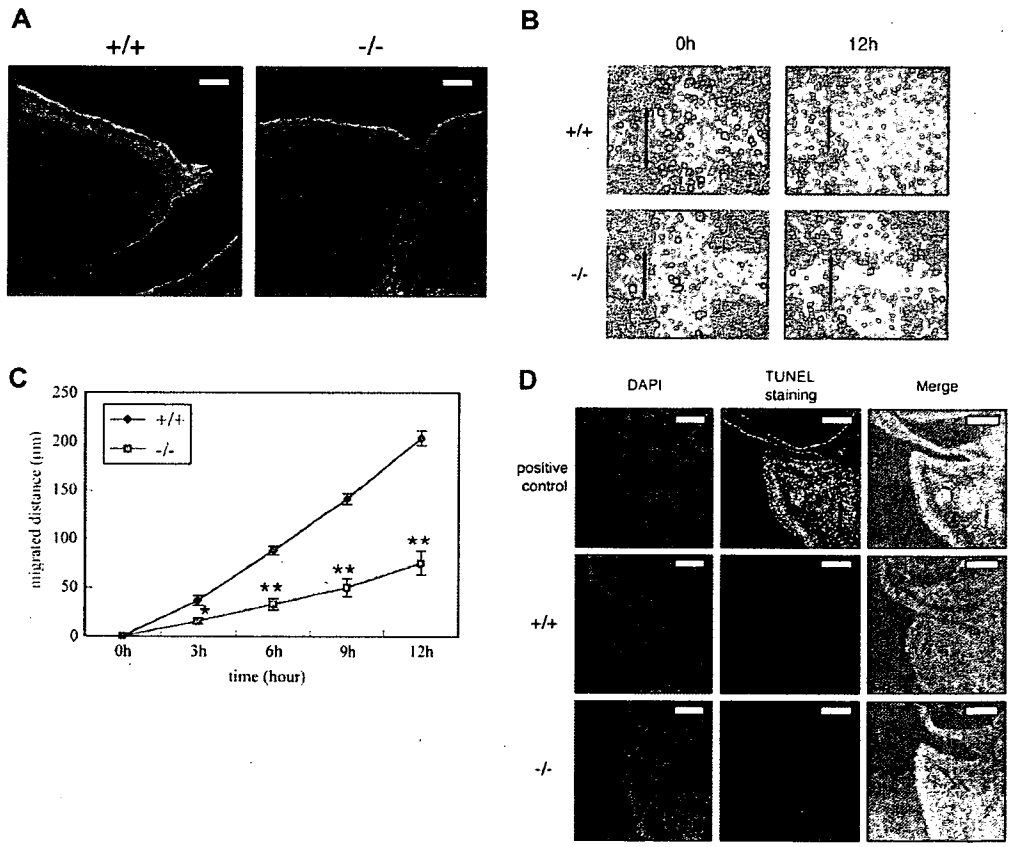

Fig. 2. EOB phenotype and impaired keratinocyte motility. (A) Coronal eye sections of E15.5 wild-type (*Lgr4* +/+) and null fetuses were stained with phalloidin-TRITC. Scale bar: 30 μm. (B) Keratinocyte motility was assessed by in vitro wound-healing scratch assay, and values representing the mean (S.E.M.; vertical bar) of 16 independent wounds are shown by a linegraph (C). (*; $P < 0.005$, **; $P < 0.001$) (D) Neither wild-type nor *Lgr4* null E15.5 fetuses showed apoptotic cells in the eyelids. Positive control is tissue treated with DNase I. Scale bar: 60 μm.

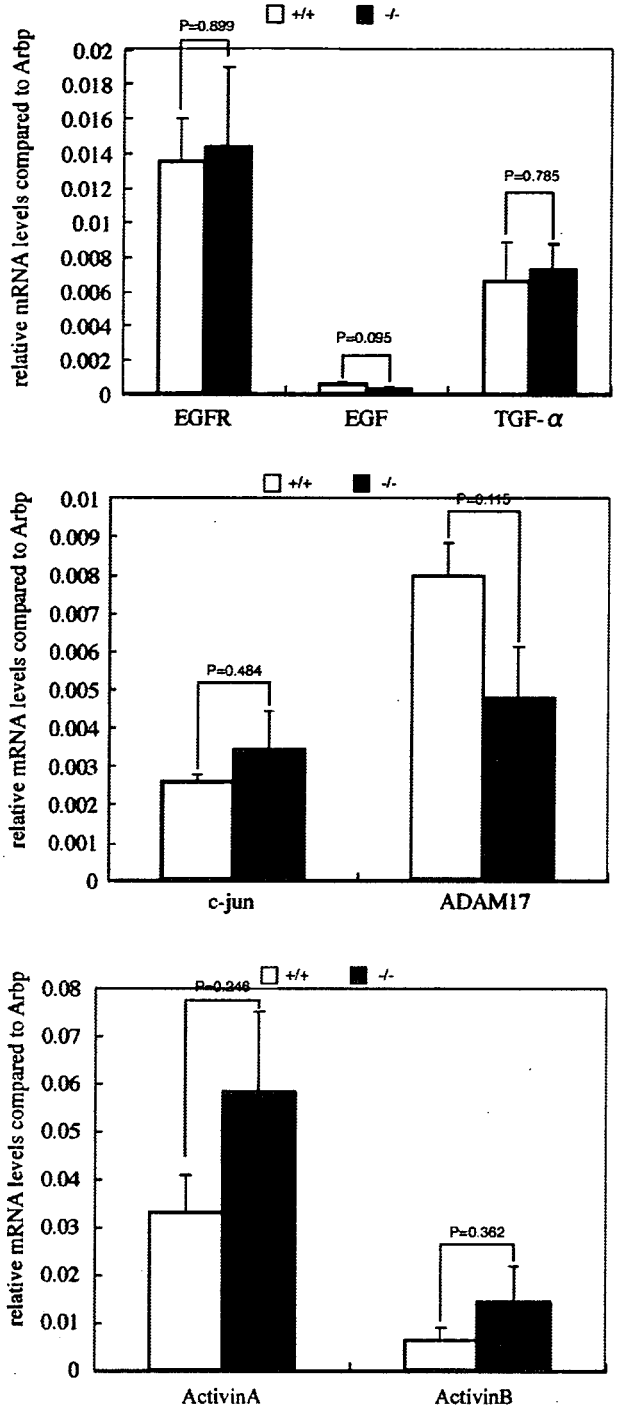

Fig. 3. Quantitative RT-PCR for cell motility-related genes. EGFR, EGF, TGF-α, c-jun, ADAM17, ActivinA and ActivinB mRNA levels in keratinocyte derived from *Lgr4* wild-type and null mice (P0) were quantified (all bars; $n = 3$). Error bars represent ± S.E.M.

(Supplementary Fig. S2A and B). The keratinocyte-specific deletion of *Lgr4* gene in *Lgr4* conditional knockout mice was confirmed by RT-PCR (Fig. 4A). The *Lgr4* conditional knockout mice were spared the embryonic/neonatal lethality (data not shown) and almost all of them showed the EOB phenotype (Fig. 4B and C). The body size and weight of several organs including the kidneys and liver were all reduced in *Lgr4* null mice [9], whereas those of the conditional knockout mice were all normal (Fig. 4D and E).

4. Discussion

In this report, we demonstrated an abnormality in the motility of keratinocytes and the EOB phenotype in *Lgr4* null mice. It is known that, during normal mouse development, the epithelial cells on the protruding tips of both the upper and lower eyelids migrate along the surface of the cornea and fuse with each other by E16.5 [12]. This suggests that EOB could be due to a defect in prenatal eyelid extension. EOB has been reported as a typical phenotype in mutant mice lacking several genes affecting epithelial cell proliferation and motility [12,13]. The genes whose deletion results in EOB include transcription factors controlling cell proliferation (c-jun [21,22]), growth factors (FGF10 [23], HB-EGF [20,24], TGF-α [25], ActivinB [26]) and their receptors (EGFR [27]), and related cytoplasmic factors functioning in signal transduction pathways (MEKK1 [28,29], JNK [30]). Xia et al. reviewed the signaling pathways required for embryonic eyelid closure in normal developmental stages and classified these into two major signaling pathways, TGFβ/activin-MEKK1-JNK/p38 and TGF-α/EGFR-ERK [13]. Our data strongly suggest that *Lgr4* plays a critical role in regulating the formation of eyelids in the embryonic stage and that it contributes to epithelial cell motility. In addition, epidermal wound-healing activity [21,27] and tumorigenesis require epithelial cell motility [29]. Although the downstream signaling mechanisms of *Lgr4* are not clear, we speculate that a novel signaling pathway exists in keratinocytes to regulate the cell motility.

We generated *Lgr4* conditional knockout mice that were spared the embryonic/neonatal lethality, reduced body weight and renal hypoplasia observed in *Lgr4* null mice, and were born with a mendelian distribution. However, almost all of these mice showed the EOB phenotype. These results strongly suggest that the keratinocyte aberration shown by *Lgr4* null mice was not induced by renal hypoplasia.

The observed impairment in keratinocyte motility may suggest that *Lgr4* controls the cell motility of keratinocytes. In this context, elucidating the precise role of *Lgr4* along with its cognate ligand would advance the knowledge of the epithelial cell motility mechanism. Interestingly, one of our *Lgr4* null mice survived for more than 40 days, showing turbid corneas in addition to various defects. Microscopic observation of the cornea showed many stripes (data not shown), and we presume that the degeneration of the cornea, including wounds, resulted from excoriation by the floor material in the cage because of the EOB. However, immunostaining of the eye tissue clearly showed positive staining at the cornea in the wild-type mice in addition to the signal at the protruding tips of the eyelid (Fig. 1B). This result also suggests the possibility that the turbid cornea observed in null mice might be caused by a deficiency of the *Lgr4* gene. Therefore, a cornea-specific deletion of *Lgr4* will be required to study further the function of *Lgr4* in the development, growth and maintenance of the cornea tissue. To our knowledge, there are no published reports of EOB caused by a deficiency of GPCR genes. In addition, in the other reports on the generation of *Lgr4* mutants (by insertion of a gene cassette carrying a splice acceptor into to an intron of

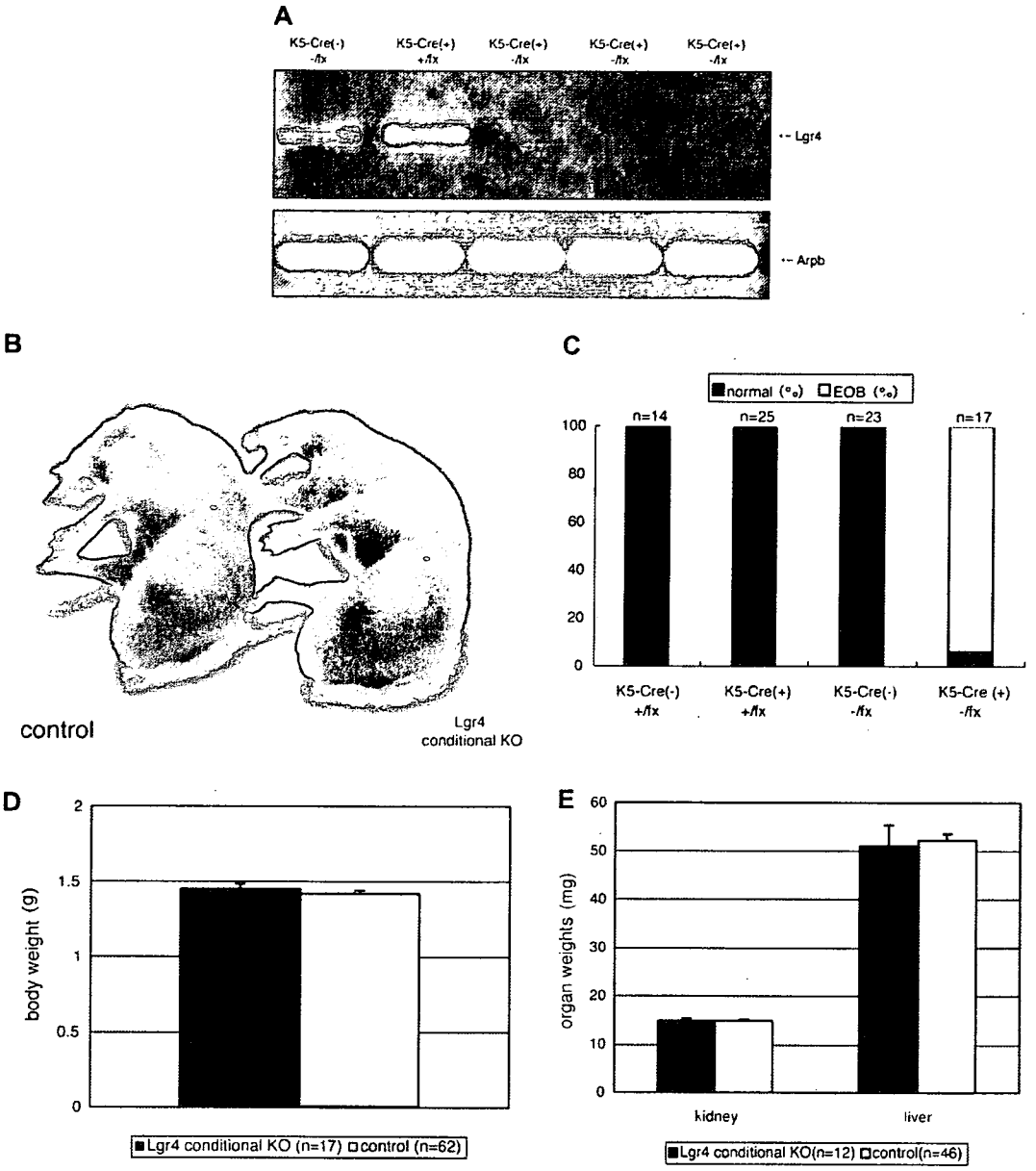

Fig. 4. Characteristics of *Lgr4* conditional knockout mice. (A) RT-PCR for *Lgr4* showed no expression of *Lgr4* mRNA in keratinocytes. Primer sets are shown in the supplementary material. (B) *Lgr4* conditional knockout mice show the typical EOB phenotype. (C) As in the case of *Lgr4* null mice, almost all of the *Lgr4* conditional knockout mice show the EOB phenotype. The body weight (D) and the organ weight of the liver and kidneys (E) of *Lgr4* conditional knockout mice are all within normal ranges.

the gene) on several genetic backgrounds [8,10,11], the EOB phenotype of the null mice was not described except in one abstract for a poster presentation [31]. Nevertheless, we predicted that *Lgr4* and its unidentified ligand(s) would likely be related to regulatory mechanisms controlling the development and maintenance of epidermal tissue including that of the eyelid.

In conclusion, we generated two mouse models, one with a complete deletion of the *Lgr4* function and another with a conditional *Lgr4* knockout, and provide evidence that *Lgr4* is involved in keratinocyte motility affecting eyelid formation. Adult conditional *Lgr4* knockout mice will be a useful tool for examining the *Lgr4* function in keratinocytes.

Acknowledgements: We would like to thank Dr. J. Takeda for providing us the K5 Cre TG mice, and Dr. M. Kitagawa for valuable discussion. This research was supported in part by a Grants-in-Aid for Exploratory Research (#17659251) from the Ministry of education, Culture, Sports, Science and Technology of Japan, and by a donation from Kureha Corporation.

Appendix A. Supplementary data

Supplementary data associated with this article can be found, in the online version, at doi:10.1016/j.febslet.2007.08.064.

References

[1] Hsu, S.Y., Liang, S.G. and Hsueh, A.J. (1998) Characterization of two LGR genes homologous to gonadotropin and thyrotropin receptors with extracellular leucine-rich repeats and a G protein-coupled, seven-transmembrane region. Mol. Endocrinol. 12, 1830–1845.

[2] Loh, E.D., Broussard, S.R., Liu, Q., Copeland, N.G., Gilbert, D.J., Jenkins, N.A. and Kolakowski Jr., L.F. (2000) Chromosomal localization of GPR48, a novel glycoprotein hormone receptor like GPCR, in human and mouse with radiation hybrid and interspecific backcross mapping. Cytogenet. Cell. Genet. 89, 2–5.

[3] Baker, P.J., Pakarinen, P., Huhtaniemi, I.T., Abel, M.H., Charlton, H.M., Kumar, T.R. and O'Shaughnessy, P.J. (2003) Failure of normal Leydig cell development in follicle-stimulating hormone (FSH) receptor-deficient mice, but not FSHbeta-deficient mice: role for constitutive FSH receptor activity. Endocrinology 144, 138–145.

[4] Huhtaniemi, I., Zhang, F.P., Kero, J., Hamalainen, T. and Poutanen, M. (2002) Transgenic and knockout mouse models for the study of luteinizing hormone and luteinizing hormone receptor function. Mol. Cell. Endocrinol. 187, 49–56.

[5] Zhang, F.P., Poutanen, M., Wilbertz, J. and Huhtaniemi, I. (2001) Normal prenatal but arrested postnatal sexual development of luteinizing hormone receptor knockout (LuRKO) mice. Mol. Endocrinol. 151, 72–183.

[6] Postiglione, M.P., Parlato, R., Rodriguez-Mallon, A., Rosica, A., Mithbaokar, P., Maresca, M., Marians, R.C., Davies, T.F., Zannini, M.S., De Felice, M. and Di Lauro, R. (2002) Role of the thyroid-stimulating hormone receptor signaling in development and differentiation of the thyroid gland. Proc. Natl. Acad. Sci. USA 99, 15462–15467.

[7] Leighton, P.A., Mitchell, K.J., Goodrich, L.V., Lu, X., Pinson, K., Scherz, P., Skarnes, W.C. and Tessier-Lavigne, M. (2001) Defining brain wiring patterns and mechanisms through gene trapping in mice. Nature 410, 174–179.

[8] Mazerbourg, S., Bouley, D.M., Sudo, S., Klein, C.A., Zhang, J.V., Kawamura, K., Goodrich, L.V., Rayburn, H., Tessier-Lavigne, M. and Hsueh, A.J. (2004) Leucine-rich repeat-containing, G protein-coupled receptor 4 null mice exhibit intrauterine growth retardation associated with embryonic and perinatal lethality. Mol. Endocrinol. 18, 2241–2254.

[9] Kato, S., Matsubara, M., Matsuo, T., Mohri, Y., Kazama, I., Hatano, R., Umezawa, A. and Nishimori, K. (2006) Leucine-rich repeat-containing G protein-coupled receptor-4 (LGR4, Gpr48) is essential for renal development in mice. Nephron Exp. Nephrol. 104, e63–e75.

[10] Mendive, F., Laurent, P., Van Schoore, G., Skarnes, W., Pochet, R. and Vassart, G. (2006) Defective postnatal development of the male reproductive tract in LGR4 knockout mice. Dev. Biol. 290, 421–434.

[11] Hoshii, T., Takeo, T., Nakagata, N., Takeya, M., Araki, K. and Yamamura, K. (2007) LGR4 regulates the postnatal development and integrity of male reproductive tracts in mice. Biol. Reprod. 76, 303–313.

[12] Xia, Y. and Karin, M. (2004) The control of cell motility and epithelial morphogenesis by Jun kinases. Trends Cell. Biol. 14, 94–101.

[13] Xia, Y. and Kao, W.W. (2004) The signaling pathways in tissue morphogenesis: a lesson from mice with eye-open at birth phenotype. Biochem. Pharmacol. 68, 997–1001.

[14] Gao, Y., Kitagawa, K., Hiramatsu, Y., Kikuchi, H., Isobe, T., Shimada, M., Uchida, C., Hattori, T., Oda, T., Nakayama, K., Nakayama, K.I., Tanaka, T., Konno, H. and Kitagawa, M. (2007) Up-regulation of GPR48 induced by down-regulation of p27Kip1 enhances carcinoma cell invasiveness and metastasis. Cancer Res. 66, 11623–11631.

[15] Keller, R. (2002) Shaping the vertebrate body plan by polarized embryonic cell movements. Science 298, 1950–1954.

[16] Sahai, E. (2005) Mechanisms of cancer cell invasion. Curr. Opin. Genet. Dev. 15, 87–96.

[17] Rodriguez, C.I., Buchholz, F., Galloway, J., Sequerra, R., Kasper, J., Ayala, R., Stewart, A.F. and Dymecki, S.M. (2000) High-efficiency deleter mice show that FLPe is an alternative to Cre-loxP. Nat. Genet. 25 (2), 139–140.

[18] Tarutani, M., Itami, S., Okabe, M., Ikawa, M., Tezuka, T., Yoshikawa, K., Kinoshita, T. and Takeda, J. (1997) Tissue-specific knockout of the mouse Pig-a gene reveals important roles for GPI-anchored proteins in skin development. Proc. Natl. Acad. Sci. USA 94, 7400–7405.

[19] Mine, N., Iwamoto, R. and Mekada, E. (2005) HB-EGF promotes epithelial cell migration in eyelid development. Development 132, 4317–4326.

[20] Shimizu, Y., Thumkeo, D., Keel, J., Ishizaki, T., Oshima, H., Oshima, M., Noda, Y., Matsumura, F., Taketo, M.M. and Narumiya, S. (2005) ROCK-I regulates closure of the eyelids and ventral body wall by inducing assembly of actomyosin bundles. J. Cell Biol. 168, 941–953.

[21] Li, G., Gustafson-Brown, C., Hanks, S.K., Nason, K., Arbeit, J.M., Pogliano, K., Wisdom, R.M. and Johnson, R.S. (2003) c-Jun is essential for organization of the epidermal leading edge. Dev. Cell. 4, 865–877.

[22] Zenz, R., Scheuch, H., Martin, P., Frank, C., Eferl, R., Kenner, L., Sibilia, M. and Wagner, E.F. (2003) c-Jun regulates eyelid closure and skin tumor development through EGFR signaling. Dev. Cell. 4, 879–889.

[23] Tao, H., Shimizu, M., Kusumoto, R., Ono, K., Noji, S. and Ohuchi, H. (2005) A dual role of FGF10 in proliferation and coordinated migration of epithelial leading edge cells during mouse eyelid development. Development 132, 3217–3230.

[24] Shirakata, Y., Kimura, R., Nanba, D., Iwamoto, R., Tokumaru, S., Morimoto, C., Yokota, K., Nakamura, M., Sayama, K., Mekada, E., Higashiyama, S. and Hashimoto, K. (2005) Heparin-binding EGF-like growth factor accelerates keratinocyte migration and skin wound healing. J. Cell. Sci. 118, 2363–2370.

[25] Luetteke, N.C., Qiu, T.H., Peiffer, R.L., Oliver, P., Smithies, O. and Lee, D.C. (1993) TGF alpha deficiency results in hair follicle and eye abnormalities in targeted and waved-1 mice. Cell 73, 263–278.

[26] Vassalli, A., Matzuk, M.M., Gardner, H.A., Lee, K.F. and Jaenisch, R. (1994) Activin/inhibin beta B subunit gene disruption leads to defects in eyelid development and female reproduction. Genes Dev. 8, 414–427.

[27] Miettinen, P.J., Berger, J.E., Meneses, J., Phung, Y., Pedersen, R.A., Werb, Z. and Derynck, R. (1995) Epithelial immaturity and multiorgan failure in mice lacking epidermal growth factor receptor. Nature 376, 337–341.

[28] Yujiri, T., Ware, M., Widmann, C., Oyer, R., Russell, D., Chan, E., Zaitsu, Y., Clarke, P., Tyler, K., Oka, Y., Fanger, G.R., Henson, P. and Johnson, G.L. (2000) MEK kinase 1 gene disruption alters cell migration and c-Jun NH2-terminal kinase regulation but does not cause a measurable defect in NF-kappa B activation. Proc. Natl. Acad. Sci. USA 97, 7272–7277.

[29] Zhang, L., Wang, W., Hayashi, Y., Jester, J.V., Birk, D.E., Gao, M., Liu, C.Y., Kao, W.W., Karin, M. and Xia, Y. (2003) A role for MEK kinase 1 in TGF-beta/activin-induced epithelium movement and embryonic eyelid closure. EMBO J. 22, 4443–4454.

[30] Weston, C.R., Wong, A., Hall, J.P., Goad, M.E., Flavell, R.A. and Davis, R.J. (2004) The c-Jun NH2-terminal kinase is essential for epidermal growth factor expression during epidermal morphogenesis. Proc. Natl. Acad. Sci. USA 101, 14114–14119.

[31] Hoshii, T., Sakumura, Y., Araki, M., Araki, K. and Yamamura, K. (2005) Analysis of abnormality in eye lid formation in LGR4 mutant mice. In: Proceedings of the 39th Annual Meeting of Japanese Society of Developmental Biologists, 1P031.

Available online at www.sciencedirect.com
ScienceDirect
Journal of Chromatography A, 1160 (2007) 263–269
JOURNAL OF CHROMATOGRAPHY A
www.elsevier.com/locate/chroma

Study on the quality control of cell therapy products Determination of *N*-glycolylneuraminic acid incorporated into human cells by nano-flow liquid chromatography/Fourier transformation ion cyclotron mass spectrometry

Noritaka Hashii [a,b], Nana Kawasaki [a,b,*], Yukari Nakajima [a,b], Masashi Toyoda [c], Yoko Katagiri [c], Satsuki Itoh [a], Akira Harazono [a], Akihiro Umezawa [c], Teruhide Yamaguchi [a]

[a] *Division of Biological Chemistry and Biologicals, National Institute of Health Sciences, 1-18-1 Kamiyouga, Setagaya-ku, Tokyo 158-8501, Japan*
[b] *Core Research for Evolutional Science and Technology (CREST) of Japan Science and Technology Agency (JST), 4-1-8 Hon-cho, Kawaguchi, Saitama 332-0012, Japan*
[c] *National Research Institute for Child Health and Development, 2-10-1 Okura, Setagaya-ku, Tokyo 157-8535, Japan*

Received 6 February 2007; received in revised form 16 May 2007; accepted 21 May 2007
Available online 25 May 2007

Abstract

N-Glycolylneuraminic acid (NeuGc), an acidic nine-carbon sugar, is produced in several animals, such as cattle and mice. Since human cells cannot synthesize NeuGc, it is considered to be immunogenic in humans. Recently, NeuGc contamination was reported in human embryonic stem cells cultured with xenogeneic serum and cells, suggesting that possibly NeuGc may harm the efficacy and safety of cell therapy products. Sialic acids have been determined by derivatization with 1,2-diamino-4,5-methylenedioxybenzene (DMB) followed by liquid chromatography/mass spectrometry (LC/MS) and liquid chromatography/tandem mass spectrometry (LC/MS/MS); however, the limited availability of cell therapy products requires more sensitive and specific methods for the quality test. Here we studied the use of nano-flow liquid chromatography/Fourier transformation ion cyclotron resonance mass spectrometry (nanoLC/FTMS) and nanoLC/MS/MS for NeuGc-specific determination at a low femtomole level. Using our method, we found NeuGc contamination of the human cell line (HL-60RG cells) cultured with human serum. Our method needs only 2.5×10^3 cells for one injection and would be applicable to the determination of NeuGc in cell therapy products.

Keywords: *N*-Glycolylneuraminic acid; Nano-flow liquid chromatography; Fourier transformation ion cyclotron mass spectrometry; Cell therapy products

1. Introduction

Sialic acids are a family of acidic nine-carbon sugars found in the non-reducing terminal of *N*-linked and *O*-linked oligosaccharides of glycoproteins and glycolipids [1,2]. There are more than 30 members with different substitutions on the amino group at carbon 5 and on hydroxyl groups at carbons 4, 7, 8 and 9 [2–8]. *N*-Glycolylneuraminic acid (NeuGc), a 5-*N*-glycolylated sialic acid, is produced in several animals, such as cattle, horses, mice and rats [9]. Since human cells cannot synthesize NeuGc due to mutation of the cytidine monophospho (CMP)-*N*-acetylneuraminic acid (NeuAc) hydroxylase gene [10,11], NeuGc is considered to be antigenic and to induce immunoreaction in humans [4,12,13].

Advances in biotechnology and cell culture techniques make it possible to administer human and animal cells directly to patients as cell therapy products. In cell therapy and tissue engineering, human embryonic stem (ES) cells are expected to be useful for the treatment of many diseases. Recently, it was reported that NeuGc is incorporated into ES cells from human and mouse feeder cells and cultivation media containing xenogeneic serum, such as fetal calf serum (FCS) [14,15]. Since NeuGc is a foreign component in humans, it is feared that NeuGc may harm the efficacy and safety of cell therapy products. To

* Corresponding author. Tel.: +81 3 3700 9074; fax: +81 3 3700 9084.
E-mail address: nana@nihs.go.jp (N. Kawasaki).

0021-9673/$ – see front matter © 2007 Elsevier B.V. All rights reserved.
doi:10.1016/j.chroma.2007.05.062

assess the adverse effects of NeuGc, it is necessary to quantify NeuGc in cell therapy products.

Sialic acids have been determined by labeling with 1,2-diamino-4,5-methylenedioxybenzene (DMB) followed by conventional high-performance liquid chromatography (HPLC) with fluorescent detection [16–20]. The femtomole level of sialic acid can be determined by fluorescent detection [19]. The use of liquid chromatography/mass spectrometry (LC/MS) and liquid chromatography/tandem mass spectrometry (LC/MS/MS) has more advantage in the identification of sialic acid species [18,20–22]. The derivatization of sialic acids with DMB has advantages of good separation of NeuGc from NeuAc in chromatography and enhancement of ionization efficiency in MS. However, more sensitive and specific methods are desired for the quality control of cell therapy products, since in many case only a low number of cell products, approximately 1×10^6 to 1×10^8, should be available for quality tests.

In this study, we studied the use of nano-flow liquid chromatography/Fourier transformation ion cyclotron resonance mass spectrometry (nanoLC/FTMS) and LC/MS/MS to achieve the sensitive and specific determination of NeuGc. The potential of the method for quality testing of cell therapy products was evaluated using substrain of human promyelocytic leukemia HL-60 cells (HL-60RG cells) as model cells. Using this method, we determined NeuGc in membrane fractions from HL-60RG cells cultured with FCS, human serum and serum-free medium.

2. Experimental

2.1. Materials

NeuGc and NeuAc were purchased from Nacalai Tesque (Kyoto, Japan). FCS and normal human serum were purchased from Dainippon Sumitomo Pharma (Osaka, Japan). RPMI1640 medium and ASF104 medium were purchased from Sigma-Aldrich (St. Louis, MO, USA) and Ajinomoto (Tokyo, Japan), respectively.

2.2. Cell culture

Substrain of human promyelocytic leukemia HL-60 cells (HL-60RG cells, JCRB Cellbank, Osaka, Japan) was cultured in RPMI1640 medium supplemented with 10% FCS, 100 unit/ml of penicillin and 100 μg/ml of streptomycin under a humidified atmosphere of 95% air and 5% CO_2 at 37 °C. HL-60RG cells were replaced at 2×10^5 cells/100 mm dish in RPMI1640 medium supplemented with 10% FCS or 10% normal human serum, and in serum-free ASF104 medium. The media were replaced four times, and semi-confluent growth cells were harvested.

2.3. Fractionation of the membrane fraction

The cells were washed in phosphate buffer saline (PBS) supplemented with protease inhibitors (protease inhibitor mix solution, Wako, Tokyo, Japan) three times. The washed cells (1×10^6) were suspended in 100 μl of 0.25 M sucrose/10 mM Tris–HCl buffer (pH 7.4) containing protease inhibitors, and sonicated at 4 °C for 30 s, two times (40W, Bioruptor UCW-201, Tosyoudenki, Kanagawa, Japan). After the nuclei were removed by centrifugation at 4 °C, 450 × *g* for 10 min, the mitochondria and lysosome fractions were removed by re-centrifugation at 4 °C, 20,000 × *g* for 10 min. The membrane fractions were precipitated by ultracentrifugation at 4 °C, 100,000 × *g* for 60 min. The membrane fractions were washed in 100 μl of 150 mM ammonium acetate buffer (pH 7.4) and recovered by re-ultracentrifugation.

2.4. Derivatization of NeuGc and NeuAc with DMB reagent

The membrane fractions were sonicated in 250 μl of H_2O and then incubated with 250 μl of 4 M acetic acid (final concentration, 2 M) at 80 °C for 3 h. The released sialic acids were passed though a solid-phase extraction cartridge (SepPak C-18, Waters, Milford, MA, USA) with 2 ml of H_2O, dried under vacuum, and resolved in 50 μl of H_2O. The solution was incubated with DMB according to the manufacturer's instruction (Takara, Tokyo, Japan), and the reaction mixture was applied on a solid-phase extraction cartridge (Envi-Carb C, Supelco, Bellefonte, PA, USA). After washing the cartridge with 2.5 ml of 5 mM ammonium acetate (pH 9.6) for desalting, the DMB-labeled sialic acids were eluted with 3 ml of 45% acetonitrile/5 mM ammonium acetate (pH 9.6). The collected fraction was freeze dried.

2.5. nanoLC/FTMS

DMB-labeled sialic acids were separated by HPLC using Paradigm MS4 (Michrom BioResource, Auburn, CA, USA) equipped with a reversed-phase C18 column (Magic C18, 50 mm × 0.1 mm, 3 μm, Michrom BioResource, Auburn, CA, USA). Elution was achieved using 0.1% formic acid/2% ace-

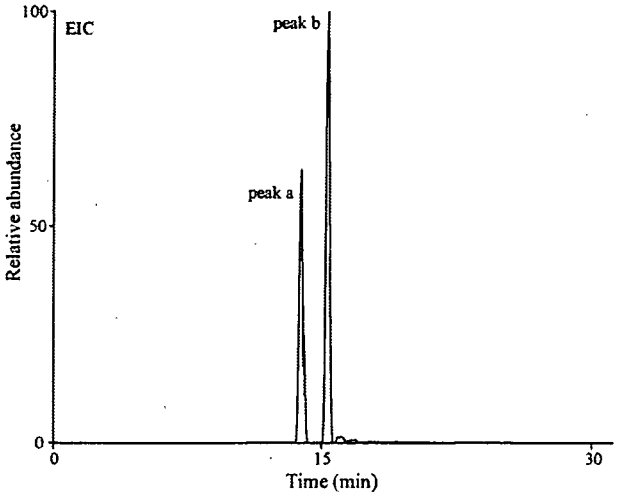

Fig. 1. EIC at *m/z* 426.13–426.17 and *m/z* 442.12–442.16 obtained by SIM (*m/z* 400–450) of DMB-NeuGc and DMB-NeuAc in the positive ion mode.

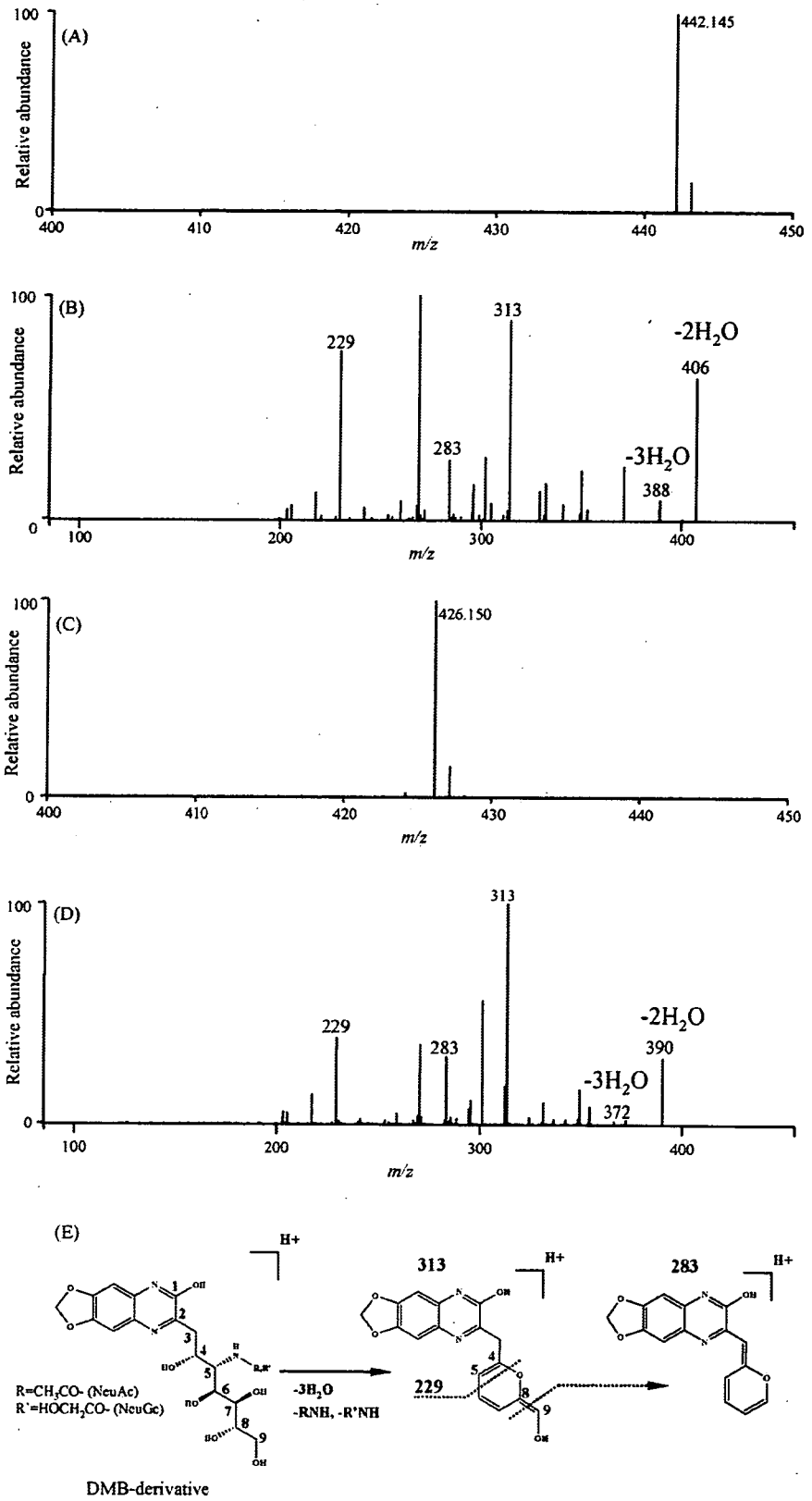

Fig. 2. (A) Typical MS spectrum of peak a. (B) MS/MS spectrum of $[M+H]^+$ (*m/z* 442.145) acquired from around peak a. (C) Typical MS spectrum of peak b. (D) MS/MS spectrum of $[M+H]^+$ (*m/z* 426.150) acquired from around peak b. (E) Fragmentation of DMB-NeuGc and DMB-NeuAc.

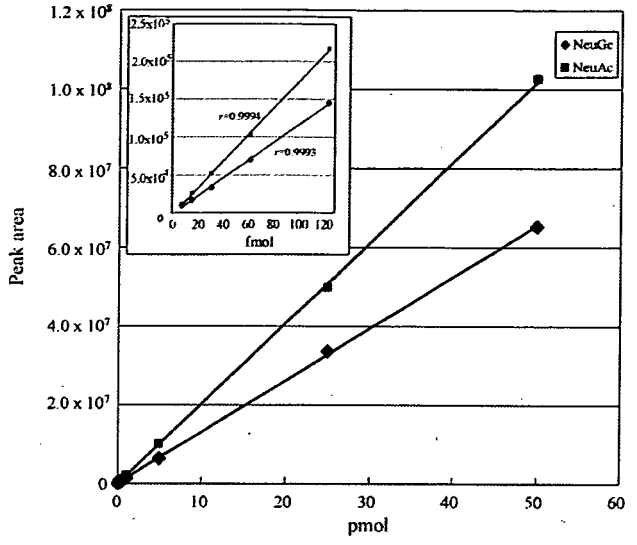

Fig. 3. Calibration curves of DMB-NeuGc ($r=0.9998$) and DMB-NeuAc ($r=0.9995$).

tonitrile (pump A) and 0.1% formic acid/80% acetonitrile (pump B) with a linear gradient of 10–90% of B in 30 min at a flow rate of 750 nl/min. On-line MS and MS/MS were performed using an Fourier transformation ion cyclotron resonance (FT)/ion trap (IT) type mass spectrometer (LTQ-FT, Thermo-Electron, San Jose, CA, USA) equipped with a nanoelectrospray ion source (AMR, Tokyo, Japan). DMB-NeuAc and DMB-NeuGc were determined by selected ion monitoring (SIM) in the positive ion mode. The analytical conditions were set to 200 °C for capillary temperature, 1800 eV spray voltage, *m/z* 400–450 scan range, and 35% collision energy. The automatic gain control (AGC) value, which is adjusted for the amount of imported ions for FTMS, was set to 5×10^4. Maximum injection times, which are the adjusted times of imported ions, for ITMS and FTMS, were set to 50 and 1250 ms, respectively.

2.6. Method validation

The linearity of the signal intensity peak area of DMB-NeuAc and DMB-NeuGc was assessed by injections of 0.0078–500 pmol DMB derivatives. Correlation coefficients were calibrated using a least-squares linear regression model. The detection limit (DL) and the quantification limit (QL) were calculated using the formulas $DL = 3.3 \times \sigma/\text{slope}$ (σ: average of noise on chromatograph) and $QL = 10 \times \sigma/\text{slope}$, respectively. Accuracy and precision were determined by measuring three samples, where NeuGc spiked at the concentration of 50 fmol to the membrane fraction of cells cultured in serum-free medium which contains no NeuGc before the derivatization of NeuGc with DMB. Accuracy was calculated by comparison of the mean peak area and the calibration curve. Precision was estimated by relative standard deviation (RSD) from three samples.

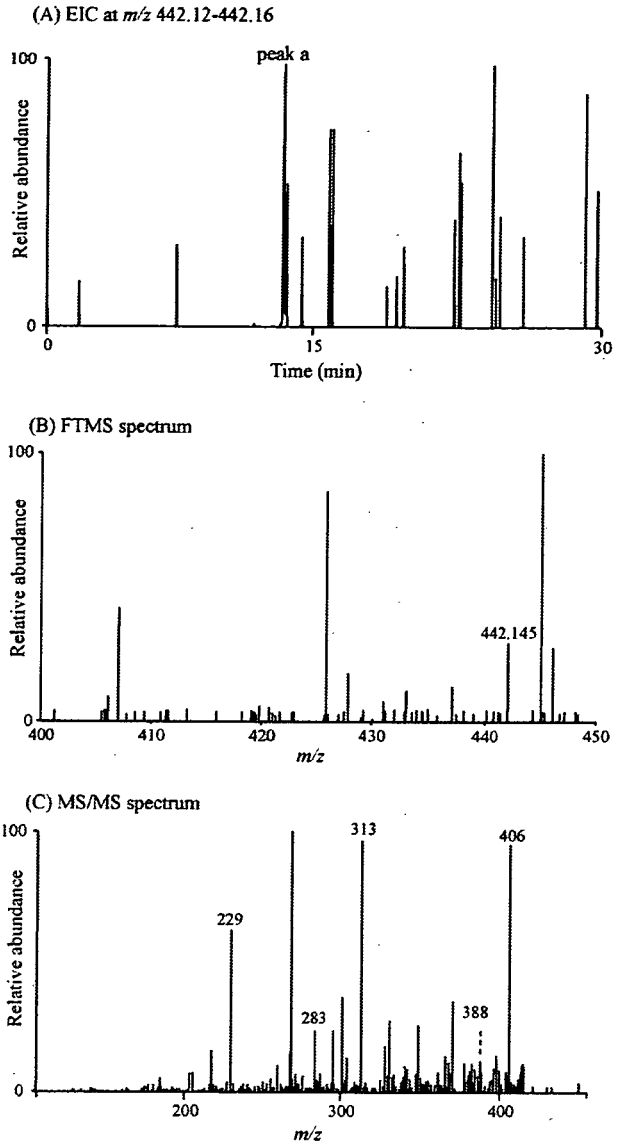

Fig. 4. Detection of DMB-NeuGc in the membrane fractions of HL-60RG cells (2.5×10^3) cultured with 10% FCS. (A) EIC at *m/z* 442.12–442.16 obtained by SIM. (B) Typical MS spectrum of peak a. (C) MS/MS spectrum of $[M+H]^+$ (*m/z* 442.145) acquired from around peak a.

3. Results and discussion

3.1. Analysis of NeuGc and NeuAc by nanoLC/FTMS

It was reported that DMB-NeuGc yielded its dehydrated ion (*m/z* 424) together with molecular ion (*m/z* 442) by MS in the positive ion mode [18,21]. To control the dehydration of molecular ion in the ion trap device, AGC value, which regulates the amount of ions trapped into ion trap device, was set to 5×10^4 (default value, 5×10^5). This value was also useful for the detection of molecular ion of DMB-NeuAc.

Using the AGC value at 5×10^4, SIM (*m/z* 400–450) was carried out in the positive ion mode. When a mix-

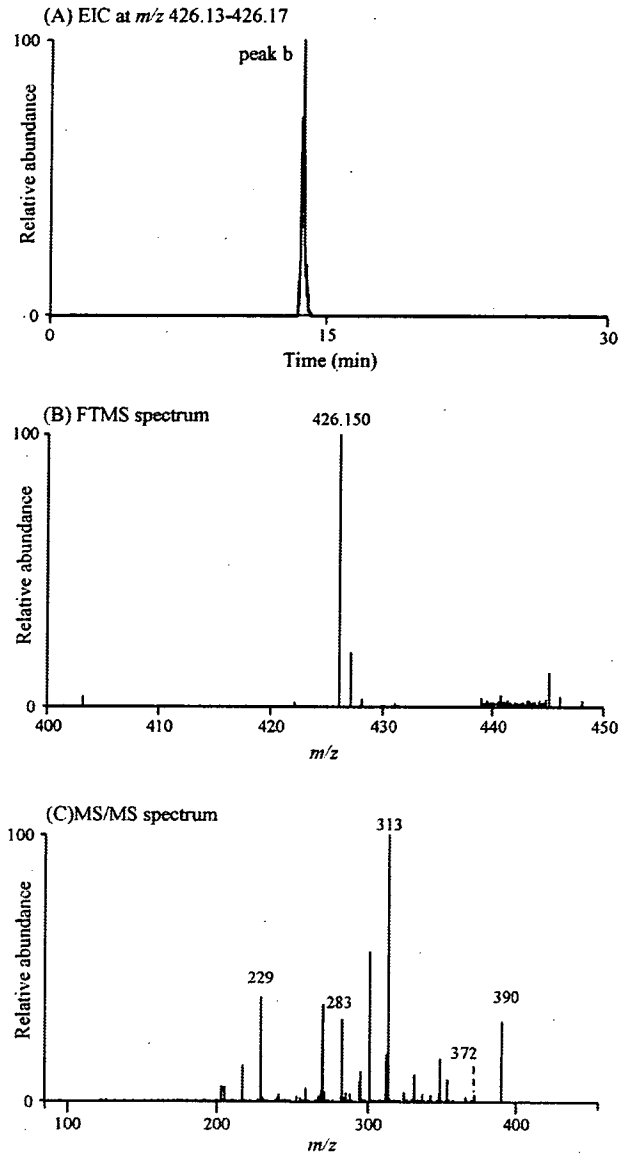

Fig. 5. Detection of DMB-NeuAc in the membrane fractions of HL-60RG cells (2.5×10^3) cultured with 10% FCS. (A) EIC at *m/z* 426.13–426.17 obtained by SIM. (B) Typical MS spectrum of peak b, (C) MS/MS spectrum of $[M+H]^+$ (*m/z* 426.150) acquired from around peak b.

ture of DMB-NeuGc and DMB-NeuAc (2 pmol each) was subjected to nanoLC/MS, two peaks appeared at 14 min (peak a) and 15 min (peak b) on the extracted ion chromatogram (EIC) at *m/z* 426.13–426.17 and *m/z* 442.12–442.16 (Fig. 1).

As shown in Fig. 2A, the *m/z* values of molecular ions around 14 min (*m/z* 442.145) suggest the elution of DMB-NeuGc in peak a. The structure of the DMB derivative at peak a was confirmed by the product ion spectra acquired from $[M+H]^+$ (*m/z* 442.145) as a precursor ion (Fig. 2B). Product ions missing two and three molecules of H_2O were found at *m/z* 406 and 388 in MS/MS spectra. Ions losing three H_2O and glycolyl groups (*m/z* 313), cross-ring fragment ion (*m/z* 229) and fragment ion

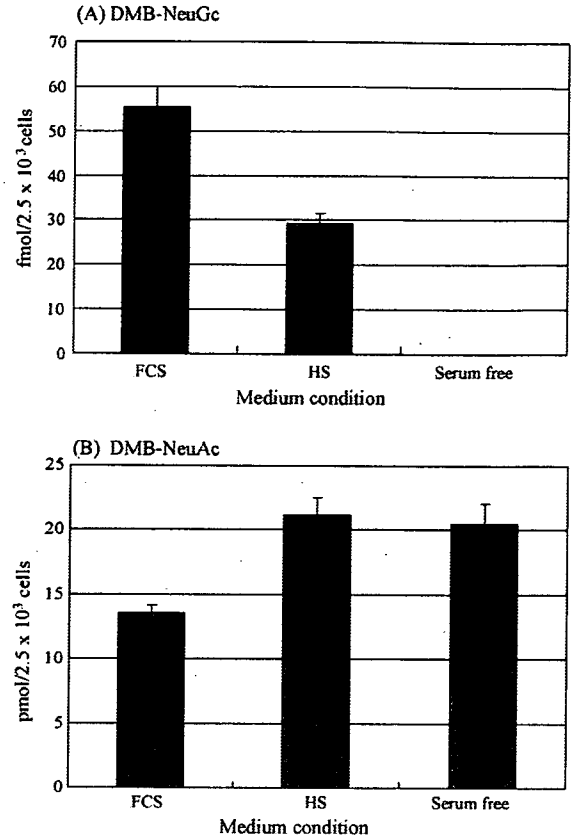

Fig. 6. Levels of (A) NeuGc and (B) NeuAc in the membrane fraction of HL-60RG cells (2.5×10^3) cultured with 10% FCS, 10% human serum (HS) and serum-free medium. Values are the means ± SD ($n = 3$).

yielded by loss of formaldehyde (*m/z* 283) were also formed by MS/MS (Fig. 2E). The fragment pattern of the MS/MS spectrum from $[M+H]^+$ (*m/z* 442.145) was consistent with that of DMB-NeuGc in the previous report [21]. Fragments at *m/z* 406 and 388 are DMB-NeuGc characteristic ions, which could be used for specific determination of DMB-NeuGc. Likewise, peak b was identified as DMB-NeuAc by molecular ions (*m/z* 426.150) and their product ions (*m/z* 390, 372, 313, 283 and 229) formed by MS/MS of $[M+H]^+$ (*m/z* 426.150) as a precursor ion (Fig. 2C and D).

Calibration curves were prepared by the injection of DMB-NeuGc and DMB-NeuAc from 0.0078 to 500 pmol. The linearity of DMB-NeuGc and DMB-NeuAc was confirmed in the range of 0.0078–50 pmol with the regression equations of $Y = 1.31 \times 10^6 X - 9028.5$ ($r = 0.9998$) and $Y = 2.03 \times 10^6 X - 21548.0$ ($r = 0.9995$), respectively (Fig. 3). DL and QL of DMB-NeuGc were 8.6 and 26.3 fmol, and those of DMB-NeuAc were 5.6 and 16.9 fmol, respectively. The use of FT/MS gave an accuracy of 92.4% by eliminating contaminants by using accurate *m/z* values. The precision of this method for NeuGc was 7.3%. Compared to the former method, in which a micro or semi-micro column and the quadrupole mass spectrometer were used for the detection of picomole levels of DMB derivatives, SIM by using nanoLC/FTMS achieved the specific detection of DMB-derivatized sialic acids at a lower level. The

method using nanoLC/FTMS and nanoLC/MS/MS allows not only the determination of DMB-derivatives with similar sensitivity as the fluorescence detection but also the identification of sialic acid species.

3.2. Quantification of NeuAc and NeuGc in membrane fraction of HL-60RG cells

Using HL-60RG cells as model cells, the potential of this method for the quantification of NeuGc on the cell membrane was evaluated. The membrane fraction from cells (1×10^6) cultured with 10% FCS was prepared by ultracentrifugation. Sialic acids were released by treatment with 2 M acetic acid at 80 °C for 3 h and derivatized with DMB. DMB derivatives (2.5×10^3 cells) were subjected to nanoLC/MS and nanoLC/MS/MS in SIM mode. As shown in Fig. 4A, some peaks appeared in EIC at *m/z* 442.12–442.16. Based on the retention time as well as the *m/z* value of molecular ion (*m/z* 442.145), peak a that appeared at 14 min was assigned to be a peak of NeuGc (Fig. 4B). Fig. 4C shows the MS/MS spectrum acquired from $[M+H]^+$ (*m/z* 442.145) as precursor. The NeuGc-characteristic ions at *m/z* 406 and 388 together with other product ions at *m/z* 313, 283 and 229 clearly indicate the presence of NeuGc in the membrane fraction of HL-60RG cells. In the EIC at *m/z* 426.13–426.17, the single peak was observed at 15 min (Fig. 5A). The molecular ion at *m/z* 426.150, and product ions at *m/z* 390, 372, 313, 283 and 229 acquired at 15.13 min suggest that DMB-NeuAc is eluted in peak b (Fig. 5B and C). The levels of NeuGc and NeuAc in the membrane fraction from HL-60RG cells (2.5×10^3 cells) cultured with 10% FCS were 55.4 ± 4.6 fmol and 13.5 ± 0.6 pmol, respectively (Fig. 6)

After the cultivation of HL-60RG cells with human serum for 10 days (medium was changed four times), NeuGc and NeuAc were determined by the proposed method. Fig. 7A shows the EIC at *m/z* 442.12–442.16 obtained by nanoLC/MS. In spite of cultivation in human serum, an obvious peak still appeared at 14 min. Molecular ion (*m/z* 442.145) and NeuGc-characteristic product ions found in the MS/MS spectrum acquired from the molecular ion clearly indicate the presence of NeuGc in the membrane fraction (Fig. 7B and C). The levels of NeuGc and NeuAc in cells (2.5×10^3) cultured in 10% human serum were 29.2 ± 2.4 fmol and 21.0 ± 1.4 pmol, respectively (Fig. 6).

In contrast, no significant peaks appeared in EIC at *m/z* 442.12–442.16 when HL-60RG cells were cultured in serum-free medium for 14 days (medium was changed four times). The level of NeuAc in cells cultured in serum-free medium was 20.5 ± 1.6 pmol (Fig. 6).

As shown in Figs. 4A and 7A, there are many different molecules detected at *m/z* 442.14–442.16 in the cells, which makes it difficult to determine a small amount of NeuGc in the membrane fraction by the low-resolution mass spectrometry. The DMB-NeuGc-specific detection was achieved by acquisition of both the accurate mass by FTMS and the characteristic product ions arisen from DMB-NeuGc by MS/MS.

Our method needs only 2.5×10^3 cells for one injection and is applicable to the determination of NeuGc in cell therapy products. The incorporation of dietary NeuGc into human serum has been reported by Tangvoranuntalul et al. [23], which has raised concerns about NeuGc contamination of cell therapy products through cultivation with human serum. Although using our method, we demonstrated the existence of NeuGc in human cells cultured with human serum, NeuGc could not be detected in human cells cultured in serum-free medium in which no NeuGc exists. These results suggest the difficulty of avoiding NeuGc contamination of cell therapy products during the manufacturing process. Further study to assess the immunogenicity of incorporated NeuGc is necessary to ensure the safety and efficacy of cell therapy products, and our method is useful for the sensitive and quantitative analysis of NeuGc in cell therapy products.

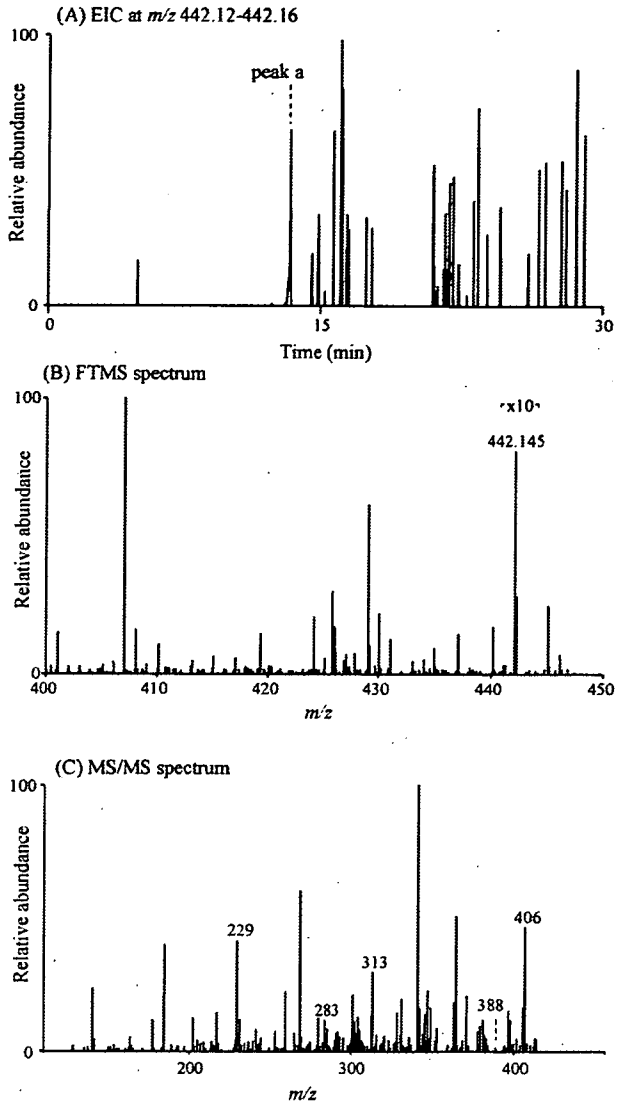

Fig. 7. Detection of DMB-NeuGc in the membrane fractions of HL-60RG cells (2.5×10^3) cultured with 10% human serum. (A) EIC at *m/z* 442.12–442.16 obtained by SIM. (B) Typical MS spectrum of peak a. (C) MS/MS spectrum of $[M+H]^+$ (*m/z* 442.145) acquired from around peak a.

Acknowledgements

This study was supported in part by a Grant-in-Aid from the Ministry of Health Labor and Welfare, and Core Research for the Evolutional Science and Technology Program, Japan Science and Technology Corp.

References

[1] C. Traving, R. Schauer, Cell Mol. Life Sci. 54 (1998) 1330.
[2] T. Angata, A. Varki, Chem. Rev. 102 (2002) 439.
[3] A. Varki, Glycobiology 2 (1992) 25.
[4] R. Schauer, Adv. Carbohydr. Chem. Biochem. 40 (1982) 131.
[5] S. Kitazume, K. Kitajima, S. Inoue, S.M. Haslam, H.R. Morris, A. Dell, W.J. Lennarz, Y. Inoue, J. Biol. Chem. 271 (1996) 6694.
[6] R. Schauer, J. Haverkamp, M. Wember, J.P. Kamerling, J.F. Vliegenthart, Eur. J. Biochem. 62 (1976) 237.
[7] N. Kawasaki, S. Itoh, M. Ohta, T. Hayakawa, Anal. Biochem. 316 (2003) 15.
[8] M. Nakano, K. Kakehi, M.H. Tsai, Y.C. Lee, Glycobiology 14 (2004) 431.
[9] E.A. Muchmore, S. Diaz, A. Varki, Am. J. Phys. Anthropol. 107 (1998) 187.
[10] A. Irie, S. Koyama, Y. Kozutsumi, T. Kawasaki, A. Suzuki, J. Biol. Chem. 273 (1998) 15866.
[11] H.H. Chou, H. Takematsu, S. Diaz, J. Iber, E. Nickerson, K.L. Wright, E.A. Muchmore, D.L. Nelson, S.T. Warren, A. Varki, Proc. Natl. Acad. Sci. U. S. A. 95 (1998) 11751.
[12] H. Higashi, M. Naiki, S. Matuo, K. Okouchi, Biochem. Biophys. Res. Commun. 79 (1977) 388.
[13] J.M. Merrick, K. Zadarlik, F. Milgrom, Int. Arch. Allergy Appl. Immunol. 57 (1978) 477.
[14] M.J. Martin, A. Muotri, F. Gage, A. Varki, Nat. Med. 11 (2005) 228.
[15] A. Heiskanen, T. Satomaa, S. Tiitinen, A. Laitinen, S. Mannelin, U. Impola, M. Mikkola, C. Olsson, H. Miller-Podraza, M. Blomqvist, A. Olonen, H. Salo, P. Lehenkari, T. Tuuri, T. Otonkoski, J. Natunen, J. Saarinen, J. Laine, Stem Cells 25 (2007) 197.
[16] A.E. Manzi, S. Diaz, A. Varki, Anal. Biochem. 188 (1990) 20.
[17] S. Hara, M. Yamaguchi, Y. Takemori, K. Furuhata, H. Ogura, M. Nakamura, Anal. Biochem. 179 (1989) 162.
[18] M. Bardor, D.H. Nguyen, S. Diaz, A. Varki, J. Biol. Chem. 280 (2005) 4228.
[19] M. Ito, K. Ikeda, Y. Suzuki, K. Tanaka, M. Saito, Anal. Biochem. 300 (2002) 260.
[20] F.N. Lamari, N.K. Karamanos, J. Chromatogr. B 781 (2002) 3.
[21] A. Klein, S. Diaz, I. Ferreira, G. Lamblin, P. Roussel, A.E. Manzi, Glycobiology 7 (1997) 421.
[22] H.H. Chou, T. Hayakawa, S. Diaz, M. Krings, E. Indriati, M. Leakey, S. Paabo, Y. Satta, N. Takahata, A. Varki, Proc. Natl. Acad. Sci. U. S. A. 99 (2002) 11736.
[23] P. Tangvoranuntakul, P. Gagneux, S. Diaz, M. Bardor, N. Varki, A. Varki, E. Muchmore, Proc. Natl. Acad. Sci. U. S. A. 100 (2003) 12045.

Progress in Hematology

International Journal of
HEMATOLOGY

Ways for a Mesenchymal Stem Cell to Live on Its Own: Maintaining an Undifferentiated State Ex Vivo

Masashi Toyoda, Hidekazu Takahashi, Akihiro Umezawa

Department of Reproductive Biology, National Institute for Child Health and Development, Tokyo, Japan

Received April 3, 2007; accepted May 2, 2007

Abstract

Like all stem cells, mesenchymal stem cells (MSC) must balance self-renewal and differentiation. Complex regulatory mechanisms are required to keep stem cells in an undifferentiated, self-renewing state and to mediate their subsequent differentiation and proliferation. In this review, we discuss how adequate numbers of MSC can be maintained in culture. In particular, we focus on identification of the cell culture conditions needed to maintain general, nonspecific potential as a stem cell over time and through replication. It would be extremely advantageous to be able to maintain MSC populations in a completely undifferentiated state and to determine and switch on specific differentiation as and when required.
Int J Hematol. 2007;86:1-4. doi: 10.1532/IJH97.07055

Key words: Mesenchymal stem cells; Cell culture; Differentiation; Cell growth; Senescence

1. Introduction

Mesenchymal stem cells (MSC) are attracting a great deal of attention, because they represent a valuable source of cells for use in regenerative medicine [1]. Use of MSC entails no ethical or immunologic problems, and they provide an excellent model of cell differentiation in biology. Not surprisingly, mesenchymal cell biology is a complex and rapidly evolving field. Critical unanswered questions remain: What defines an MSC (as opposed to just a mesenchymal cell), and what provides MSC with their unique properties?

Stem cell biology is based on the principle that any tissue may contain cells that possess the potential for both self-renewal and differentiation into one or more cell types. Mesenchymal cells are derived from an organ's supporting tissue, as opposed to parenchyma or the supporting framework of an animal organ, which typically consists of connective tissue. Among these cells exist stem cells, which have two basic processes, ie, self-renewal and differentiation. MSC were first discovered in 1976 by Friedenstein, who described clonal, plastic-adherent cells from bone marrow that provided a physical scaffold for hematopoiesis and that could differentiate into osteoblasts, chondrocytes, and adipocytes in vitro [2]. To date, investigators have demonstrated that MSC per se can be recovered from a variety of adult tissues and have the capacity to differentiate into a variety of specific cell types [3-8]. The mesenchymal phenotype can be maintained under optimal culture conditions, and MSC in vitro are recognized as adherent fibroblastic cells with a generally spindle shape, although some candidate populations of cells are more spherical with few spindle-shaped cells [9]. This heterogeneous population is too "crude" to consist solely of MSC. Although MSC can be harvested from a variety of tissues and have multipotency (ie, the capability to differentiate into numerous tissue lineages, including myoblasts, cardiomyocytes, osteoblasts, adipocytes, chondrocytes, and possibly even neural cells), MSC populations cannot easily be induced to differentiate into one lineage at the same time. There are some cell populations that behave like progenitor cells with monopotency or bipotency. In this review, we describe how MSC derived from a variety of tissues have tissue-specific characteristics and discuss optimal culture conditions that can allow the cells both to keep proliferating in an undifferentiated, self-renewing state and to permit mediation of their future differentiation.

Correspondence and reprint requests: Akihiro Umezawa, Department of Reproductive Biology, National Institute for Child Health and Development, 2-10-1, Okura, Setagaya-ku, Tokyo, 157-8535, Japan; 81-3-5494-7047 (e-mail: umezawa@1985.jukuin.keio.ac.jp).

2. MSC Optimally Require Their Original Milieu

Stem cells are indispensable entities in most multicellular organisms in that they are responsible for forming tissues during early development and for maintaining them in the adult stage. Because all somatic stem cells, including MSC, have the same genetic material, every cell type has the potential to express a stem cell phenotype under specific conditions; that is, tissue-specific flexibility is inherent. Mesenchymal cells, of which connective tissue is mainly composed, do not develop into a tissue or an organ. The cells synthesize the extracellular matrix by themselves and in vitro establish favorable environments for growth. Mesenchymal cell cultures can be made from suspensions of cells dissociated from tissues, and microscopical and biochemical analyses facilitate exploration of the effects of adding or removing specific molecules, such as hormones or growth factors.

Cells vary in their needs in a cell type–specific manner, and cells can therefore be categorized or defined by their requirements. Bone marrow–derived MSC, for example, can be compared with umbilical cord blood–derived MSC. Several methods are available for distinguishing between these two types of cells. One such method is flow cytometric analysis of markers that appear on the surfaces of the cells. Some surface marker characteristics of bone marrow–derived MSC are the same as those of cord blood–derived MSC (eg, $CD29^+$, $CD44^+$, $CD55^+$, $CD59^+$, $CD34^-$, and $CD117^-$ [10-12]). On the other hand, the CD90 and CD133 markers can be used to distinguish cord blood–derived cells from bone marrow–derived cells, because these markers are expressed in multipotent marrow-derived cells but not in cord blood–derived cells [12]. As yet, no surface markers have been identified that define MSC. Another method is complementary DNA microarray/chip technology. Because of the logical connection between gene expression and cell function, gene expression patterns can predict the variation in cell phenotypes and reveal novel phenotypic aspects of the cells and tissues studied. In mesenchymal cell culture, expression of genes encoding growth factor receptors is an important factor in microarray analysis–based investigations of the effects of growth factors, because cells dissociated from different tissues, such as bone marrow and cord blood, have different responses to growth factors (Table 1). This response affects differentiation potential. Bone marrow–derived cells can differentiate into osteoblasts, chondrocytes, cardiomyocytes, adipocytes, skeletal myocytes, and neural cells and do so according to the specific cell culture conditions, whereas cord blood–derived cells exhibit only osteogenic and adipogenic potential under the same conditions.

How can the microenvironment, culture conditions, or growth factors dictate the identity of MSC and their production of different progeny? Serum plays a critical role in the growth of cells in vitro by providing components such as amino acids, lipids, growth factors, vitamins, hormones, and attachment factors, by acting as a pH buffer, and by providing protease inhibitors. Most media for mesenchymal cell culture include a poorly defined mixture of macromolecules in the form of fetal calf serum; however, the use of serum for MSC culture makes it difficult to know which specific macromolecules a particular type of cell requires for survival and normal function. This difficulty led to the development of serum-free chemically defined media. In addition to the usual molecules, such specialized media will need to contain essential growth factors that the MSC require in culture. The primary requirements of MSC in culture reflect the origin of the cells; that is, investigators have to try to recreate the specific native tissue/organ milieu of the cells' origin. Identification of a means to create an "Elysium" or ideal stress-free native environments for cultivating and maintaining MSC will bestow significant benefits for future stem cell therapeutics.

3. The Paradox of Cell Growth versus Life Span

In cell culture it is important not only to remove animal serum from the culture medium (for reasons of medical safety with respect to infectious diseases [13-15]) but also to obtain large numbers of cells for use in therapy. Cells must be propagated in vitro to obtain the large numbers needed for biomedical procedures; however, Hayflick's problem is unavoidable in normal cells [16,17]. Most vertebrate cells stop dividing after a finite number of divisions in culture, a process called *senescence* [17,18]. Senescence is classified into two categories: "stress-induced premature senescence" (or "telomere-independent senescence") and "replicative senescence" (or "telomere-dependent senescence") [19-21]. Marrow-derived mesenchymal cells divide approximately 25 to 40 times [11,22] in culture before they cease dividing or reach senescence (M0, mortality stage 0, ie, premature senescence), whereas a few cells that overcome this step restart proliferation but stop dividing again in replicative senescence (M1) (Figure 1).

To resolve these problems, investigators can extend the life span of bone marrow–derived MSC via retroviral transduction of human telomerase reverse transcriptase (hTERT) and human papillomavirus type 16 E6 and/or E7 genes [11]. A significant observation is that an increase in telomerase

Table 1.
Reactivities of Mesenchymal Stem Cells to Growth Factors*

	MSC	UCB	UE6E7T-12	UE7T-13
PDGF	+++	+++	+++	+++
EGF	+++	++	+++	++
aFGF	+++	++	++	+
bFGF	+++	+++	+++	++
LIF	–	+	++	+
VEGF	+	+	+	–
HGF	–	–	+	–
IGF-1	+	+	–	–
IL-1	–	–	–	++
IL-6	–	–	+	–

*Plus and minus symbols show the strength of growth factor reactivity based on cell proliferation. MSC indicates human bone marrow–derived mesenchymal stem cells; UCB, human umbilical cord blood–derived mesenchymal stem cells; UE6E7T-12 and UE7T-13, MSC transduced with human papillomavirus type 16 E6 and/or E7, and human telomerase reverse transcriptase (hTERT); PDGF, platelet-derived growth factor; EGF, epidermal growth factor; aFGF, acidic fibroblast growth factor; bFGF, basic FGF; LIF, leukemia inhibitory factor; VEGF, vascular endothelial growth factor; IGF-1, insulin-like growth factor 1; IL-1, interleukin 1.